Crystallization Conditions and Mineral Chemistry in the East of Tafresh, Central Iran, with Insights into Magmatic Processes

Davood RAEISI[1] and Hassan MRNEJAD[1, 2, *]

[1] *Department of Geology, Faculty of Science, University of Tehran, Tehran, Iran*
[2] *Department of Geology and Environmental Earth Sciences, Miami University, Oxford, Ohio, USA*

Abstract: The Tafresh granitoids are located at the central part of the Urumieh-Dokhtar Magmatic Arc (UDMA) in Iran. These rocks, mainly consisting of diorite and granodiorite, were emplaced during the Early Miocene. They are composed of varying proportions of plagioclase + K-feldspar + hornblende ± quartz ± biotite. Discrimination diagrams and chemical indices of amphibole phases reveal a calc-alkaline affinity and fall clearly in the crust-mantle mixed source field. The estimated pressure, derived from Al in amphibole barometry, is approximately 3 Kb. The granitoids are I-type, metaluminous and belong to the calc-alkaline series. They are all enriched in light rare earth elements and large ion lithophile elements, depleted in high field strength elements and display geochemical features typical of subduction-related calc-alkaline arc magmas. Most crystal size distribution (CSD) line patterns from the granitoids show a non-straight trend which points to the effect of physical processes during petrogenesis .The presence of numerous mafic enclaves, sieve texture and oscillatory zoning along with the CSD results show that magma mixing in the magma chamber had an important role in the petrogenesis of Tafresh granitoids. Moreover, the CSD analysis suggests that the plagioclase crystals were crystallized in a time span of less than 1000 years, which is indicative of shallow depth magma crystallization.

Key words: crust-mantle mixed source, I-type, subduction, crystal size distribution, magma mixing, Urumieh-Dokhtar Magmatic Arc

Citation: Raeisi et al., 2019. Crystallization Conditions and Mineral Chemistry in the East of Tafresh, Central Iran, with Insights into Magmatic Processes. Acta Geologica Sinica (English Edition), 93(6): 1755–1772. DOI: 10.1111/1755-6724.13878

1 Introduction

The behavior of magma in the chamber is controlled by different factors such as: temperature, pressure, chemistry, oxygen fugacity, etc., the variations of any of which will affect the texture of the resultant rock. Therefore, the texture of an igneous rock is a remarkable recorder of igneous processes (Van der Zwan et al., 2013; Viccaro et al., 2006).

As igneous rocks crystallize, there occurs a complex interplay of crystal nucleation and growth. Whether in relatively quickly cooled volcanic rocks and shallow intrusions, or in slowly cooled plutonic rocks, these changes are recorded in their textures. A key to understanding the formation of igneous rocks is to read and interpret their crystal chemical compositions and textures (Renzulli and Santi, 1997; Jerram and Cheadle, 2000; Kuşcu and Floyd, 2001). Quantitative analyses of textures (i.e., crystal size, form, orientation, and association) are a basis for understanding the physical characteristics of magma crystallization (Higgins, 2006; Mock et al., 2003; Marsh, 1988; Jerram and Higgins, 2007). Analysis of CSD, introduced by Randolph and Larson (1988), is a quantitative petrographic technique (e.g., Higgins, 1988; 2006; 2011) that consists of plotting the natural logarithm of the population density (n) *vs.* crystal length (L) (Castro et al., 2004). In general, as crystal size increases, population density decreases. A typical CSD plot is a linear, or gently curved array with a negative slope (Cashman and Marsh, 1988; Marsh, 1988; 1998; Higgins, 1996; 2000; 2002). Analytical expressions of crystal size, population density and crystal volume can be derived from the regression trend of the CSD array, as discussed by many authors (e.g., Cashman and Marsh, 1988; Cashman, 1990; Higgins, 1994; 2000; 2006; Mock and Jerram, 2005; Jerram and Higgins, 2007; Pourkhorsandi et al., 2015).

In this study, the CSD technique is used to provide insight into the relative roles of residence time, textural coarsening, magma mixing, and renewed magma injection during cooling of Miocene granitoids in the Tafresh granitoids of the Urumieh-Dokhtar Magmatic Arc (UDMA), central Iran.

The principal objective of this study is to explore the mineralogical evidence that provides insight into potential magma mixing/mingling processes in the Tafresh granitoids. The Tafresh granitoids, of Miocene age, immediately followed widespread Eocene magmatic activity. Tafresh diorite (20.1 mya) and granodiorite (19.4 mya) (Mirnejad et al., 2018) are I-type granitoids similar

* Corresponding author. E-mail: hmirnejad@ut.ac.ir

to several other intrusive rocks of the UDMA. To get insights to the preceding questions, we tried to quantify the textural information and mineral chemistry recorded in these granitoids with an emphasis on crystal size distributions of plagioclase, which is ideal for this purpose because of the abundance and wide compositional variation of plagioclase.

2 Geological Background and Petrography

Tafresh granitoids are situated in the UDMA 24 km to the east of the city of Tafresh (Fig. 1). Igneous emplacement was associated with the northward subduction of the Neo-Tethys oceanic crust beneath the Iranian continental plate (Stöklin, 1968; Berberian et al., 1982; Alavi, 1994). Deposition of felsic to intermediate volcanics (Agard et al, 2011) was followed by the main plutonic activity (emplacement of batholiths and porphyritic stocks) during the Eocene, 55–36 my ago (Verdel et al., 2011). The volcanic rocks near Tafresh consist of rhyolite, dacite, andesite and basalt, which are locally interbedded with sediments. These sediments contain shallow marine fossils, and display textures suggestive of submarine eruption (Hajian, 2001).

Tafresh granitoids occupy a 11×5 km area, trending generally E-W, extending from Sarbadan to Ghahan (Fig. 2). Intrusive and sub-volcanic bodies of diorite to granodiorite, with blocky and massive structures, are in contact with younger sedimentary units and Eocene volcanic rocks (Fig. 2).

The Sarbadan 5×4.5 km body, mostly granodiorite, has a medium-grained and granular texture that consists of plagioclase (45–50%), K-feldspar (30–35%), quartz (10–20%), biotite (5–10%) and hornblende (5–10%) (Fig. 3a, b). Accessory minerals are opaque minerals (2–3%), pyroxene, zircon and titanite (1–2%). Plagioclase forms euhedral to subhedral and tabular crystals (0.2 to 2.7 mm) with optical zonation (Fig. 3a) and sieve texture (Fig. 3b). Most of the quartz occurs as small interstitial grains (0.1 to 0.64 mm). Orthoclase ranges from 0.3 to 2.2 mm in size (Fig. 3a). Idiomorphic amphibole grains are scattered within a feldspar and quartz matrix. Amphibole crystals, from 2.5 to 0.1 mm, show poikilitic textures containing plagioclase ± opaque minerals (Fig. 3c).

The Ghahan 4×5 km igneous body consists of diorite and lesser quantities of quartz diorite, having a sub-granular to granular texture (Fig. 3d). The minerals present are mainly amphibole, plagioclase, ± alkali feldspar, ± quartz (Fig. 3d). Plagioclase (65–85%) is mostly idiomorphic to hypidiomorphic, and elongated (3.12–0.13 mm). Some plagioclase crystals exhibit sieve texture (Fig. 3e). Orthoclase (10–20%) occurs as euhedral to anhedral crystals (1.2-0.2 mm), partly altered to sericite. The groundmass is composed of intergranular fine-grained (0.6

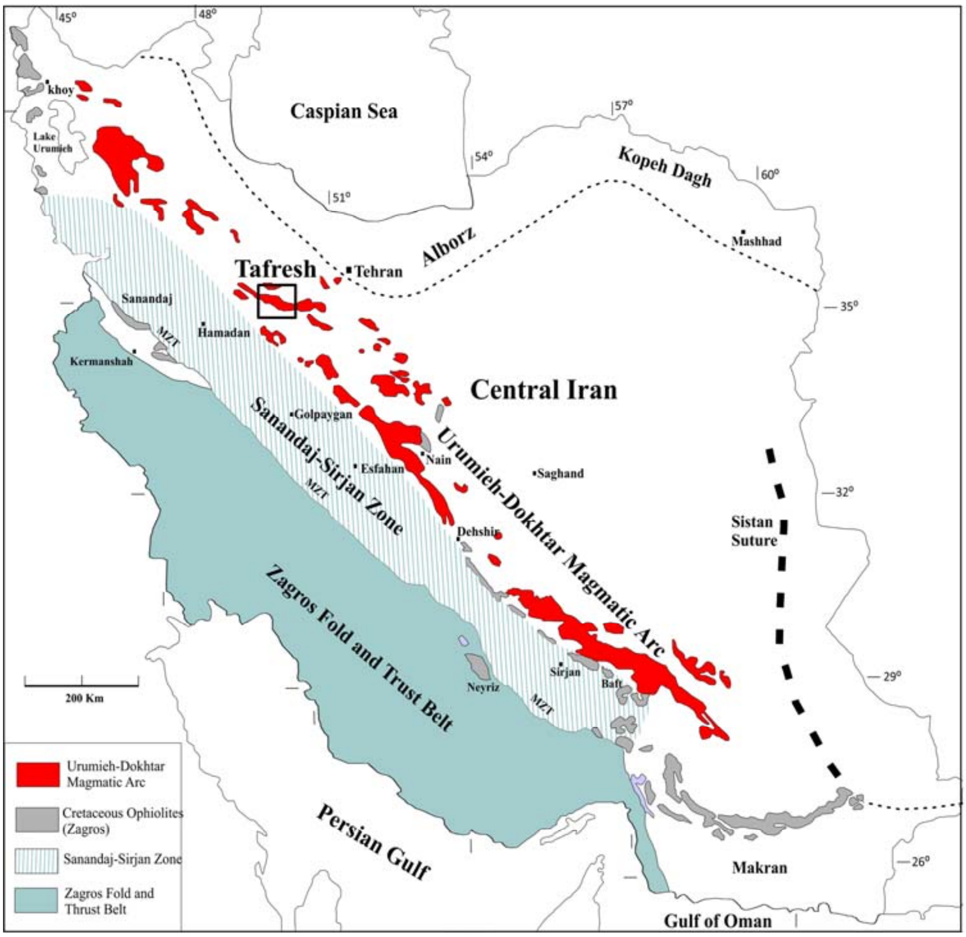

Fig. 1. Simplified geological map of Iran (Aghanabati, 2004).

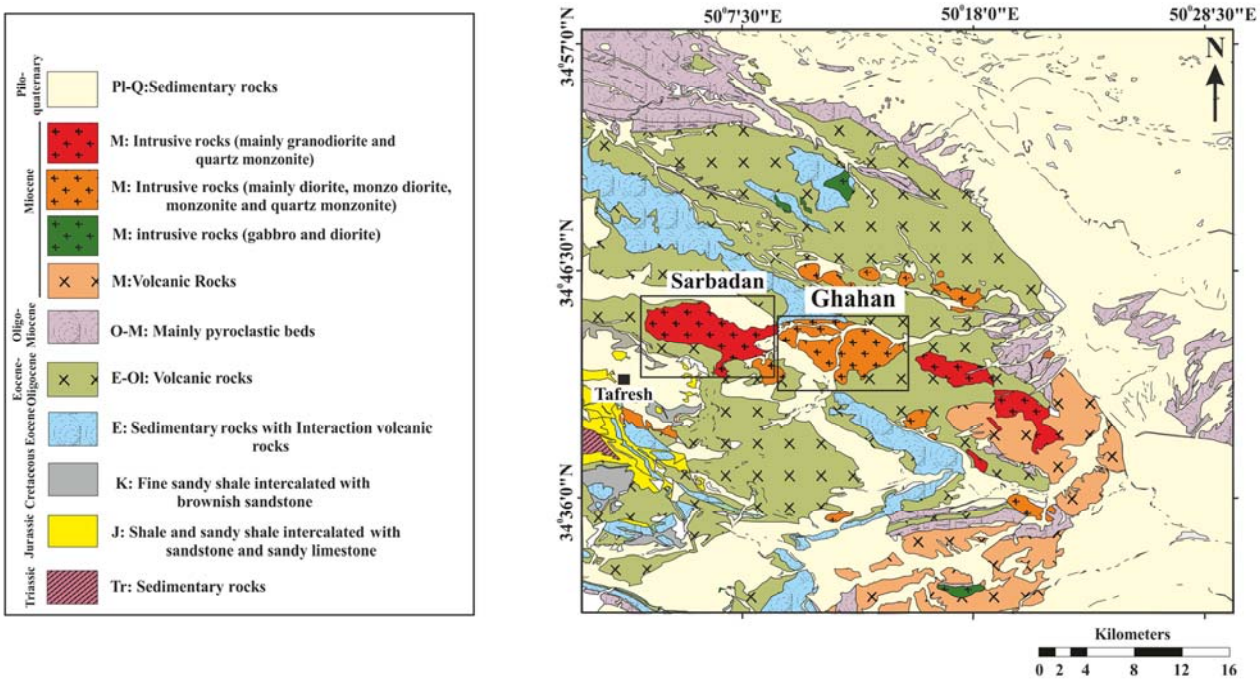

Fig. 2. Simplified geological map of the Tafresh area (Hajian, 2001). Ghahan and Sarbadan stocks are indicated by a dark box.

–0.1 mm) quartz (5–15%) (Fig. 3a, b). Amphibole (5–15%) occurs as euhedral to subhedral phenocrysts (3.6–0.2 mm) partially altered to chlorite and with a poikilitic texture (Fig. 3d). Sporadic opaque minerals (2–5%) occur as small grains (0.01-0.4 mm) either in the groundmass, or as inclusions in larger crystals.

Independent and agglomerated globular or elliptical microgranular mafic enclaves (MMEs) are locally abundant and occur throughout the Tafresh granitoids. The Tafresh granitoids contain many independent and agglomerated globular or elliptical microgranular mafic enclaves (MMEs) that are dark colored in hand-specimens. These enclaves display sharp contacts with the host MMEs in the Tafresh granitoids showing common magmatic textures and are ellipsoidal, with sizes ranging from 0.5 to 5 cm, and sharp contacts against the host granitoid (Fig. 4). Petrographically, the MMEs are fine-grained and display distinctive mineral assemblages that are fine grained, and mainly consist of plagioclase and amphibole (Fig. 4). The groundmass consists of plagioclase (65–75%), hornblende (10–15%), orthoclase (5–10%) and subordinate amounts of opaque minerals (2–5%). Euhedral crystals of plagioclase enclose small rounded hornblende grains. Typically, subhedral hornblende ranges from 0.3 to 0.7 mm. The accessory minerals, including epidote, apatite laths, and titanite, are observable in most granitoid samples .The presence of acicular apatite and plagioclase crystals with oscillatory zoning, and resorption surfaces from mixing textures can be interpreted as other non-equilibrium textures in the studied rocks (e.g., Barbarin, 1990; Hibbard, 1991, 1995).

3 Analytical Methods

Electron microprobe analysis of amphibole and plagioclase grains was done at the Iranian Mineral Processing Research Center using a CAMECA SX 100 equipped with a wavelength-dispersive spectrometer (WDS). The accelerating voltage was 15 kV, with a beam current of 20 nA and a 0–2 μm focused electron beam. The data were corrected using a modified ZAF correction procedure (Fialin, 1988). The precision of the method for major elements was <0.5% of the measured concentration. Tables 1–3 provide representative amphibole and plagioclase analyses. The beam sizes used for phenocrysts and matrix were 3 μm and 1 μm, respectively. The natural and synthetic standards used were minerals of known compositions included albite (Na), periclase (Mg), corundum (Al), wollastonite (Ca, Si), orthoclase (K), pyrophanite (Mn, Ti) and magnetite (Fe). Counting times were 10–30 s for peaks and 10 s for background. Analytical accuracy varies between 1 and 5 % depending on the abundance of the element.

Following petrographic studies, 6 fresh samples were selected for geochemical analysis by inductively coupled plasma optical emission spectroscopy (ICP-OES) at the Department of Geology and Environmental Earth Sciences, Miami University, USA. During preparation, 50 mg of a sample powder was fused with 75 mg $LiBO_2$ and dissolved in 125 ml of 0.3 N HNO_3. Repeated analyses established a precision of ±1% for major elements, and ±5% for most trace elements (Table 4).

Eight thin sections were selected for quantitative optical microscopy and CSD studies. Mosaic images were obtained at the CEREGE Institute, Aix-Marseille University (France) for identification of the typology and estimation of mineral abundance and size. Measured parameters included length, width, area and crystal orientation. The mosaic images were a basis on which to draw precise images of plagioclase crystals in preparation

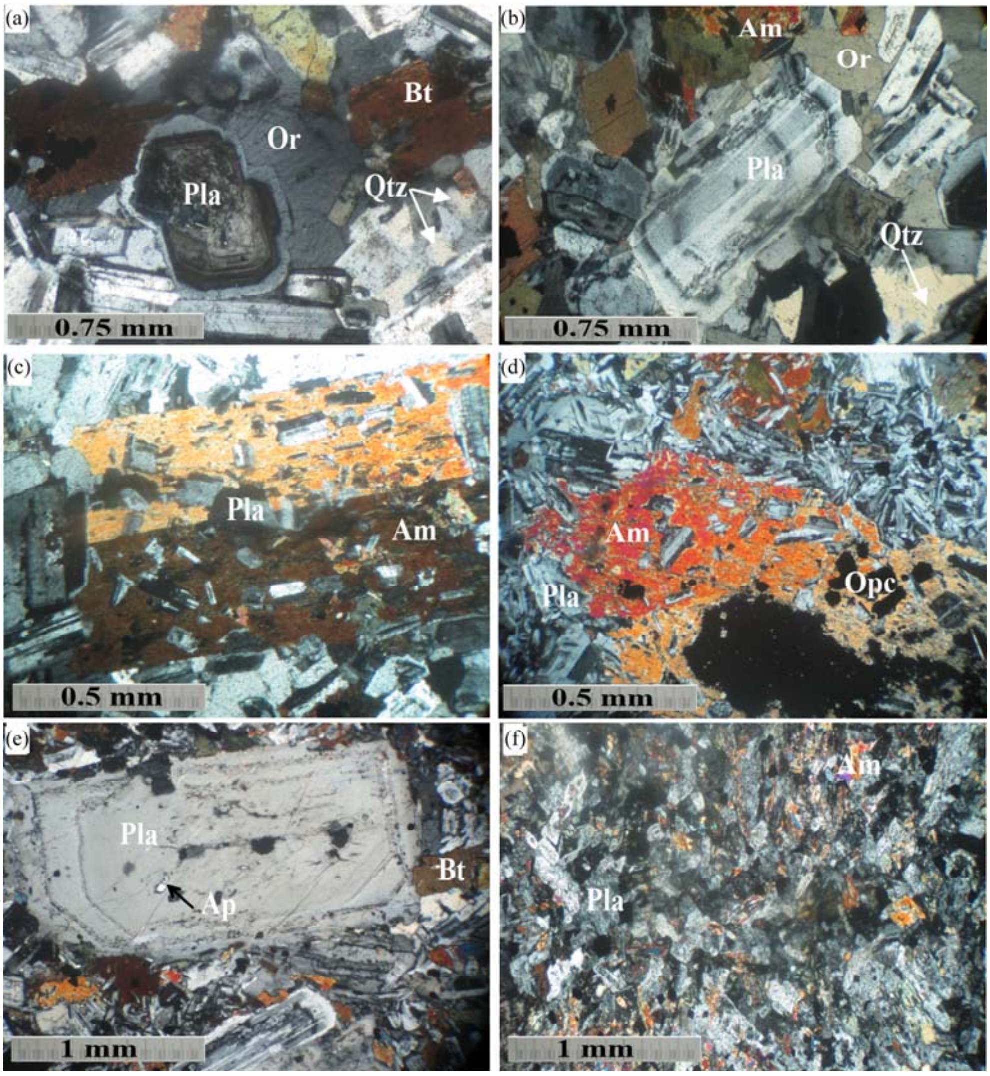

Fig. 3. (a) Granular granitoid rock in Ghahan region. Plagioclase crystals are associated with alkali feldspar, quartz, amphibole, and opaque minerals; (b) euhedral plagioclase with sieve texture; (c, d) Poikilitic amphibole (plagioclase inclusions); (e) plagioclase phenocrysts with oscillatory zoning and sieve texture; (f) fine grain microdiorite enclaves.

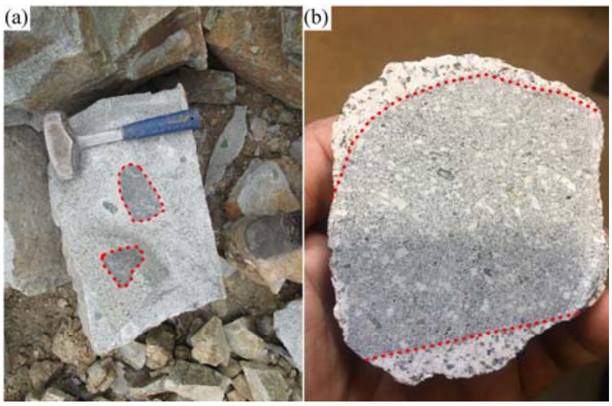

Fig. 4. (a, b) Fine-grained microdiorite enclaves in diorite.

for the measurement of crystal length and width using ImageJ and JMicroVision 1.2.7 software. The procedure was monitored by continual comparison with optical images and direct microscopic investigation. Finally, the 3-D characteristics of the crystals were compared with the crystal size distribution diagram, the frequency of the width-to-length ratio of the crystals, and these were compared to the diagrams from the CSDSlice5 Spreadsheet (Morgan and Jerram 2006).

The obtained data were added to a CSD Corrections 1.4.0 software environment to draw CSD diagrams. The input of CSD Corrections requires values on intersection lengths of the crystals, area of the measured thin section, crystal roundness, rock fabric and crystal habit.

As proposed by Marsh (1988), the average value for crystal residence time is calculated by employing the equation:

$$n=n_0\exp(-L/Gt)$$

where $n=dN/dL$; n refers to the total number of crystals smaller than L and L is the crystal size in each span. G is the average rate of linear growth, t is the average time for the presence of the crystal in the system and n_0 refers to

Table 1 Representative electron microprobe analyses of amphiboles from the Ghahan and Sarbadan granitoids(wt%)

Sample		SiO_2	Al_2O_3	TiO_2	FeO	MnO	MgO	CaO	Na_2O	K_2O	NiO	P_2O_5	Total	No. of oxygens	TSi	Mg /(Mg+Fe2)	(Ca+Na) (B)	Na (B)	Al t	Al vi	Al iv	Fe/ (Fe+Mg)	log fO2
Ghahan	Gh1	49.3	6.2	1.5	11.9	0.4	14.9	11.5	1.3	0.6	0.0	0.0	97.5	23.0	7.1	0.8	2.0	0.2	1.1	0.2	0.9	0.3	−12.8
	Gh2	49.3	6.4	1.4	11.9	0.4	15.0	11.5	1.1	0.7	0.0	0.1	97.8	23.0	7.1	0.8	2.0	0.2	1.1	0.2	0.9	0.3	−12.6
	Gh3	49.9	6.3	1.4	12.0	0.5	14.8	11.4	1.7	0.8	0.0	0.0	98.6	23.0	7.1	0.7	2.0	0.3	1.1	0.2	0.9	0.3	−12.9
	Gh4	49.3	5.6	1.1	13.7	0.6	14.3	11.5	1.2	0.6	0.0	0.0	97.9	23.0	7.1	0.7	2.0	0.2	1.0	0.1	0.9	0.3	−13.1
	Gh5	48.6	5.7	1.5	13.6	0.5	13.5	12.5	1.2	0.6	0.0	0.0	97.8	23.0	7.1	0.6	2.0	0.0	1.0	0.1	0.9	0.4	−13.2
	Gh6	48.4	6.0	1.2	13.6	0.5	14.2	12.4	1.3	0.6	0.0	0.0	98.2	23.0	7.0	0.7	2.0	0.1	1.0	0.1	1.0	0.3	−12.7
	Gh7	49.5	5.8	1.3	14.5	0.6	13.4	12.7	0.0	0.6	0.0	0.0	98.3	23.0	7.2	0.7	2.0	0.0	1.0	0.1	0.8	0.4	−13.4
	Gh8	50.7	5.3	0.9	11.7	0.6	16.6	11.6	1.1	0.4	0.0	0.0	98.9	23.0	7.1	0.9	2.0	0.3	0.9	0.0	0.9	0.3	−12.3
	Gh9	51.5	4.6	0.9	11.1	0.6	16.8	11.6	0.9	0.3	0.0	0.1	98.4	23.0	7.2	0.9	2.0	0.2	0.8	0.0	0.8	0.3	−12.8
	Gh10	52.3	4.6	0.9	11.2	0.6	17.1	11.9	0.9	0.4	0.0	0.0	100.0	23.0	7.2	0.9	2.0	0.2	0.8	0.0	0.8	0.3	−12.8
	Gh11	47.6	7.5	1.6	12.1	0.6	16.3	11.2	1.8	0.3	0.0	0.0	99.1	23.0	6.7	0.9	2.0	0.3	1.2	0.0	1.2	0.3	−10.6
	Gh12	48.5	7.0	1.2	12.0	0.5	17.5	10.6	1.9	0.3	0.0	0.0	99.5	23.0	6.7	1.0	1.9	0.4	1.1	0.0	1.1	0.3	*
	Gh13	50.8	4.5	0.9	10.7	0.7	19.3	10.9	1.0	0.4	0.0	0.0	99.2	23.0	7.0	1.0	1.9	0.3	0.7	0.0	0.7	0.2	*
	Gh14	49.3	5.7	1.2	12.1	0.7	16.5	11.2	1.3	0.5	0.0	0.0	98.5	23.0	7.0	0.9	2.0	0.3	0.9	0.0	0.9	0.3	−11.2
	Gh15	51.1	4.8	1.0	10.8	0.7	18.4	11.1	1.1	0.4	0.0	0.0	99.4	23.0	7.0	1.0	1.9	0.3	0.8	0.0	0.8	0.2	*
	Gh16	51.3	4.7	0.9	11.2	0.7	19.2	10.9	1.0	0.4	0.0	0.0	100.2	23.0	7.0	1.0	1.9	0.3	0.8	0.0	0.8	0.2	*
	Gh17	51.4	4.5	1.0	11.3	0.8	17.7	11.3	1.0	0.4	0.0	0.0	99.2	23.0	7.1	1.0	1.9	0.3	0.7	0.0	0.7	0.3	*
	Gh18	49.7	6.1	1.2	11.7	0.7	17.1	11.1	1.3	0.2	0.0	0.0	99.1	23.0	6.9	1.0	2.0	0.3	1.0	0.0	1.0	0.3	−10.9
	Gh19	51.2	4.9	0.9	11.0	0.6	18.5	10.9	1.1	0.4	0.0	0.0	99.5	23.0	7.0	1.0	1.9	0.3	0.8	0.0	0.8	0.3	*
	Gh20	52.0	6.1	1.5	11.7	0.5	15.4	11.3	1.5	0.4	0.0	0.0	100.4	23.0	7.2	0.8	2.0	0.3	1.0	0.2	0.8	0.3	*
	Gh21	51.4	6.1	1.7	13.4	0.5	14.2	11.4	1.5	0.6	0.0	0.1	100.7	23.0	7.2	0.7	2.0	0.3	1.0	0.2	0.8	0.3	*
	Gh22	50.1	5.7	1.0	11.9	0.7	15.7	11.2	4.1	0.4	0.0	0.0	100.7	23.0	7.1	0.7	2.0	0.3	1.0	0.1	0.9	0.3	−12.6
	Gh23	49.2	5.9	1.0	12.0	0.7	15.4	11.3	1.6	0.5	0.0	0.0	97.5	23.0	7.1	0.8	2.0	0.3	1.0	0.1	0.9	0.3	−12.5
	Gh24	49.8	5.5	0.9	11.8	0.8	15.6	10.8	1.7	0.3	0.0	0.0	97.2	23.0	7.1	0.8	2.0	0.3	0.9	0.1	0.9	0.3	−12.8
	Gh25	49.4	5.7	1.1	11.6	0.5	15.5	11.4	1.4	0.5	0.0	0.0	97.1	23.0	7.1	0.8	2.0	0.2	1.0	0.1	0.9	0.3	−12.6
	Gh26	48.4	6.6	1.2	11.9	0.6	15.2	10.8	1.5	0.4	0.0	0.0	96.5	23.0	7.0	0.8	2.0	0.3	1.1	0.1	1.0	0.3	−12.3
	Gh27	49.5	5.2	1.0	12.3	0.7	15.6	11.3	3.3	0.4	0.0	0.0	99.4	23.0	7.1	0.7	2.0	0.3	0.9	0.0	0.9	0.3	−12.6
Sarbadan	Sa1	49.4	5.4	1.3	14.2	0.6	14.1	11.7	1.2	0.5	0.0	0.0	98.5	23.0	7.1	0.7	2.0	0.2	0.9	0.0	0.9	0.4	−13.3
	Sa2	48.8	5.4	1.4	13.7	0.6	14.5	11.9	1.2	0.6	0.0	0.1	98.1	23.0	7.1	0.7	2.0	0.2	0.9	0.0	0.9	0.3	−12.8
	Sa3	48.9	6.3	1.6	13.3	0.5	14.0	11.5	1.3	0.6	0.0	0.0	98.0	23.0	7.1	0.7	2.0	0.2	1.1	0.1	0.9	0.3	−13.0
	Sa4	46.8	6.0	1.5	13.3	0.4	15.6	12.4	1.4	0.5	0.0	0.1	98.0	23.0	6.8	0.8	2.0	0.1	1.0	0.0	1.0	0.3	−10.1
	Sa5	44.6	7.4	1.0	16.4	0.6	11.1	12.0	1.2	0.9	0.0	0.0	95.2	23.0	6.8	0.6	2.0	0.0	1.3	0.2	1.2	0.5	*
	Sa6	49.8	5.4	1.3	13.8	0.6	14.3	12.2	1.1	0.5	0.0	0.0	99.1	23.0	7.1	0.7	2.0	0.1	0.9	0.1	0.9	0.4	−13.2
	Sa7	49.3	5.4	1.6	13.7	0.5	14.7	12.3	1.2	0.5	0.0	0.0	99.2	23.0	7.1	0.7	2.0	0.1	0.9	0.0	0.9	0.3	−12.8
	Sa8	49.6	5.6	1.5	12.8	0.5	14.6	11.4	1.4	0.4	0.0	0.0	97.7	23.0	7.2	0.7	2.0	0.2	1.0	0.1	0.8	0.3	−13.2
	Sa9	49.8	5.1	0.9	12.8	0.7	15.0	11.5	0.8	0.4	0.0	0.1	97.0	23.0	7.2	0.8	2.0	0.2	0.9	0.0	0.8	0.3	−13.0

Table 2 Representative electron microprobe analyses of plagioclase from the Ghahan granitoids (wt%)

Sample	No.	SiO_2	TiO_2	Al_2O_3	FeO	MnO	MgO	CaO	Na_2O	K_2O	NiO	P_2O_5	Total	Or	Ab	An
Gh	1	54.75	0.01	29.10	0.34	0.01	0.07	11.12	3.99	0.21	0.00	0.01	99.61	2.15	40.88	56.97
Gh	2	55.15	0.03	29.16	0.35	0.02	0.01	11.09	4.31	0.22	0.00	0.00	100.34	2.18	42.78	55.04
Gh	3	55.24	0.02	28.94	0.31	0.00	0.00	10.65	4.21	0.21	0.02	0.01	99.61	2.15	43.20	54.64
Gh	4	55.55	0.00	28.25	0.26	0.00	0.00	12.06	4.46	0.19	0.01	0.01	100.79	2.40	46.35	51.25
Gh	5	56.41	0.04	28.40	0.31	0.00	0.02	9.88	4.71	0.27	0.02	0.01	100.07	2.72	47.48	49.80
Gh	6	46.18	0.00	34.34	0.35	0.00	0.13	17.47	1.80	0.05	0.00	0.02	100.34	0.47	17.01	82.52
Gh	7	50.48	0.01	31.50	0.33	0.00	0.02	13.11	4.58	0.15	0.00	0.01	100.19	1.33	40.58	58.09
Gh	8	44.58	0.02	35.80	0.48	0.02	0.00	17.13	1.66	0.05	0.00	0.00	99.74	0.49	16.16	83.36
Gh	9	57.72	0.04	26.96	0.22	0.00	0.00	8.71	4.65	0.31	0.00	0.03	98.64	7.13	16.15	76.72
Gh	10	56.72	0.05	26.72	0.47	0.01	0.06	10.13	4.20	0.11	0.02	0.02	98.51	0.47	17.01	82.52
Gh	11	63.06	0.00	20.97	0.18	0.00	0.00	8.07	5.90	0.21	0.00	0.01	98.40	1.33	40.58	58.09
G1	Core to rim	49.78	1.13	5.81	13.34	0.55	14.60	11.57	1.29	0.57	0.00	0.02	98.66	7.46	16.87	75.67
G1		49.50	1.34	6.03	13.40	0.61	14.06	11.36	1.37	0.63	0.00	0.02	98.32	8.20	17.84	73.96
G1		62.04	0.00	23.59	0.13	0.01	0.00	5.75	7.12	0.35	0.01	0.00	99.00	1.14	30.70	68.16
G1		56.09	0.01	27.74	0.33	0.00	0.04	10.88	3.91	0.22	0.01	0.01	99.24	3.04	42.48	54.48
G1		38.34	3.95	13.75	17.28	0.26	12.96	0.01	0.00	9.74	0.00	0.00	96.29	2.44	49.39	48.17
G1		51.80	0.00	32.35	0.27	0.01	0.01	12.22	2.51	0.10	0.02	0.00	99.29	3.10	50.91	45.99
G1		54.24	0.00	28.39	0.25	0.00	0.00	13.17	3.67	0.19	0.02	0.01	99.94	4.32	58.16	37.52
G2	Core to rim	48.77	1.25	6.85	13.14	0.50	14.82	11.29	0.68	0.64	0.00	0.00	97.94	9.19	9.76	81.05
G2		49.88	1.17	5.63	12.73	0.51	14.75	11.40	1.20	0.53	0.00	0.00	97.80	7.13	16.15	76.72
G2		52.15	0.02	31.20	0.35	0.00	0.04	13.65	3.11	0.17	0.00	0.02	100.71	1.68	30.78	67.54
G2		56.27	0.01	28.86	0.34	0.01	0.05	10.48	4.44	0.22	0.01	0.04	100.73	2.22	44.85	52.93
G2		56.51	0.01	28.54	0.35	0.01	0.05	10.19	4.21	0.24	0.01	0.01	100.13	2.51	44.11	53.38
G2		52.76	0.02	30.69	0.35	0.01	0.00	13.10	2.95	0.11	0.00	0.04	100.03	1.14	30.70	68.16
G2		57.21	0.02	28.38	0.31	0.01	0.00	9.70	4.60	0.26	0.00	0.05	100.54	2.68	47.37	49.95
G2		57.76	0.02	27.34	0.33	0.00	0.07	8.89	4.92	0.30	0.00	0.00	99.63	3.10	50.91	45.99
G2		58.12	0.01	27.42	0.25	0.00	0.00	8.80	5.21	0.31	0.00	0.00	100.12	3.13	52.52	44.35
G3	Core to rim	55.79	0.01	27.84	0.26	0.00	0.00	10.52	4.36	0.25	0.01	0.00	99.04	1.99	39.21	58.81
G3		56.28	0.00	29.33	0.19	0.01	0.00	10.12	4.53	0.23	0.02	0.00	100.71	2.34	46.13	51.53
G3		56.23	0.01	29.14	0.24	0.01	0.00	10.24	4.63	0.24	0.02	0.02	100.78	2.40	46.35	51.25
G3		56.88	0.01	28.71	0.26	0.00	0.08	9.46	4.85	0.24	0.00	0.05	100.54	2.44	49.39	48.17
G3		56.51	0.02	29.23	0.28	0.00	0.08	9.04	4.84	0.25	0.03	0.02	100.30	2.60	50.36	47.03
G3		60.38	0.02	26.65	0.21	0.00	0.03	7.29	5.65	0.42	0.00	0.00	100.65	4.32	58.16	37.52
G4	Core to rim	55.27	0.00	26.94	0.18	0.00	0.04	10.28	4.03	0.27	0.03	0.03	97.07	1.68	30.78	67.54
G4		54.08	0.02	29.64	0.36	0.01	0.03	11.85	3.95	0.20	0.01	0.00	100.15	1.99	39.21	58.81
G4		56.03	0.03	28.48	0.38	0.00	0.04	10.03	3.91	0.28	0.03	0.01	99.22	3.04	42.48	54.48
G4		56.24	0.01	27.56	0.17	0.00	0.02	10.25	4.09	0.24	0.01	0.00	98.59	2.22	44.85	52.93
G4		56.57	0.01	27.65	0.29	0.01	0.00	11.59	4.21	0.23	0.00	0.00	100.56	2.60	50.36	47.03
G4		54.77	0.01	28.06	0.28	0.01	0.00	11.46	3.78	0.20	0.02	0.03	98.62	2.15	40.88	56.97
G4		63.36	0.05	24.34	0.21	0.00	0.05	5.11	7.35	0.31	0.00	0.04	100.82	2.15	43.20	54.64
G4		53.56	0.02	28.87	0.38	0.01	0.00	11.70	3.63	0.21	0.00	0.02	98.40	2.72	47.48	49.80
G4		65.68	0.01	22.50	0.19	0.00	0.01	3.82	6.93	0.65	0.00	0.00	99.79	4.23	65.53	30.25

nucleation density at a point where L reaches 0. Nucleation rate J is calculated through $n_0=J/G$ in which n_0 is a constant quantity which is obtained from the intersection of the cumulative density axis of crystal size.

This equation is equal to:

$$Tr = (-1/G\times m)/31{,}536{,}000$$

where Tr is the residence time (years), G is the growth rate of crystals (mm/s), m is the slope of the CSD curve of the log-linear data, and the 31,536,000 coefficient converts seconds to years.

4 Results

4.1 Whole-rock chemistry

The bulk-rock chemical data (Table 4) were plotted in a variety of standard petrological diagrams (Fig. 5). Accordingly, the Ghahan/Sarbadan suite is characterized as diorite or granodiorite (Fig. 5a), calc-alkalic (Fig. 5b), metaluminous (Fig. 5c), I-type (Fig. 5d), with a volcanic arc affinity (Fig. 5e). In a diagram of mantle-normalized (Fig. 5f) abundances of selected major and trace elements, data from the two localities are slightly offset, but track quite closely.

4.2 Mineral chemistry

4.2.1 Amphibole

Amphiboles from the Ghahan and Sarbadan localities show a narrow range of compositional variation. Structural formulas, calculated on an anhydrous basis assuming 23 oxygen atoms per half unit cell, place them in the calcic group (magnesio-hornblende) according to the classification scheme of Leake et al. (2004) (Fig. 6a). In a (Na + Ca + K) *vs.* Si diagram, which discriminates between metamorphic and igneous amphiboles, all data fall decisively in the igneous field, (Fig. 6b). In the TiO_2 *vs.* Al_2O_3 diagram, data for all the amphibole crystals plot in the crust-mantle mixed source field (Fig. 6c).

4.2.2 Plagioclase

Plagioclase, the most common phase, mainly occurs as an isolated euhedral to subhedral tabular crystal. The anorthite component decreases from diorite ($An_{30\text{-}83}$) to

Table 3 Representative electron microprobe analyses of plagioclase from the Sarbadan granitoids (wt%)

Sample	No.	SiO_2	TiO_2	Al_2O_3	FeO	MnO	MgO	CaO	Na_2O	K_2O	NiO	P_2O_5	Total	Or	Ab	An
Sa	1	54.45	0.02	28.51	0.26	0.02	0.19	9.54	7.57	0.26	0.00	0.04	100.86	2.06	60.08	37.86
Sa	2	60.39	0.04	24.37	0.15	0.00	0.05	6.91	8.32	0.56	0.02	0.00	100.81	4.54	67.45	28.01
Sa	3	52.55	0.00	30.16	0.28	0.00	0.06	10.64	6.98	0.21	0.01	0.00	100.89	1.68	55.80	42.53
Sa	4	53.36	0.00	29.70	0.27	0.00	0.00	10.98	5.71	0.25	0.01	0.02	100.30	2.18	49.87	47.95
Sa	5	55.88	0.02	27.34	0.26	0.00	0.08	8.13	8.76	0.33	0.01	0.00	100.81	2.51	66.59	30.90
Sa	6	62.73	0.02	22.63	0.19	0.00	0.00	5.76	6.40	0.35	0.00	0.02	98.10	2.28	53.53	44.19
Sa	7	59.83	0.04	24.88	0.31	0.01	0.02	8.85	4.16	0.25	0.00	0.00	98.35	3.29	62.11	34.60
Sa	8	56.77	0.00	26.61	0.34	0.00	0.01	10.43	4.58	0.30	0.00	0.01	99.05	2.80	59.87	37.32
Sa	9	65.97	0.05	18.85	0.09	0.00	0.00	0.07	1.07	13.01	0.01	0.01	99.13	3.15	62.88	33.97
Sa	10	57.15	0.05	27.48	0.14	0.01	0.00	9.79	4.73	0.19	0.00	0.02	99.56	2.44	52.26	45.30
Sa	11	66.73	0.03	18.63	0.14	0.02	0.00	0.35	1.80	10.80	0.00	0.00	98.50	2.06	60.09	37.85
Sa	12	66.38	0.00	19.53	0.06	0.00	0.00	0.01	0.31	12.68	0.00	0.00	98.97	1.75	56.78	41.47
Sa	13	55.46	0.07	25.05	0.39	0.01	0.02	9.12	4.31	0.22	0.00	0.06	94.71	2.36	65.52	32.11
Sa	14	60.96	0.07	23.51	0.21	0.01	0.00	9.55	4.41	0.26	0.01	0.00	98.99	2.51	50.89	46.61
Sa	15	65.98	0.04	18.71	0.10	0.00	0.01	0.03	0.73	13.98	0.00	0.00	99.58	3.02	65.26	31.72
Sa	16	56.03	0.00	27.32	0.19	0.01	0.01	10.13	6.12	0.31	0.01	0.04	100.17	1.71	51.33	46.95
Sa	17	58.04	0.01	26.26	0.17	0.00	0.00	8.70	6.33	0.42	0.00	0.00	99.93	2.42	55.46	42.12
Sa	18	58.05	0.01	25.97	0.16	0.00	0.00	8.38	7.05	0.45	0.00	0.02	100.09	2.47	58.86	38.66
Sa	19	57.54	0.03	26.19	0.20	0.00	0.00	8.17	6.79	0.36	0.00	0.01	99.29	2.05	58.83	39.12
Sa	20	58.96	0.00	25.84	0.20	0.01	0.00	7.99	7.45	0.41	0.01	0.00	100.87	2.22	61.39	36.38
Sa	21	57.10	0.02	26.80	0.18	0.01	0.00	9.60	5.93	0.33	0.01	0.04	100.02	1.90	51.78	46.32
Sa	22	56.70	0.02	27.34	0.15	0.00	0.01	10.01	6.47	0.25	0.00	0.04	100.99	1.35	53.18	45.47
Sa	23	55.47	0.00	28.35	0.18	0.00	0.00	10.70	5.90	0.26	0.00	0.00	100.86	1.43	49.23	49.34
Sa	24	56.55	0.01	26.19	0.18	0.01	0.00	9.25	7.77	0.38	0.00	0.02	100.36	1.90	59.17	38.93
Sa	25	55.99	0.00	26.97	0.19	0.00	0.00	9.85	7.49	0.33	0.02	0.01	100.85	1.65	56.96	41.39
Sa	26	59.03	0.01	25.62	0.21	0.00	0.02	8.18	7.32	0.43	0.00	0.03	100.85	2.33	60.38	37.29
Sa	27	58.73	0.01	27.46	0.20	0.00	0.00	9.61	4.47	0.27	0.02	0.00	100.77	3.84	62.12	34.04
Sa	28	59.13	0.01	27.17	0.19	0.02	0.00	9.07	5.04	0.29	0.00	0.01	100.93	3.28	65.57	31.15
Sa	29	61.66	0.01	23.90	0.14	0.00	0.00	5.89	8.11	0.52	0.00	0.00	100.23	2.92	69.28	27.80
Sa	30	57.55	0.01	26.72	0.17	0.01	0.00	9.04	6.91	0.35	0.01	0.03	100.80	1.90	56.94	41.16
G5	Core to rim	57.81	0.03	27.53	0.30	0.01	0.12	9.91	4.63	0.28	0.00	0.02	100.64	2.84	46.93	50.23
G5		57.50	0.02	28.14	0.31	0.01	0.10	9.48	4.71	0.26	0.00	0.05	100.58	2.68	48.51	48.82
G5		56.96	0.00	28.14	0.31	0.00	0.14	9.49	5.10	0.30	0.00	0.00	100.44	2.96	50.27	46.77
G5		54.81	0.00	27.67	0.19	0.01	0.01	10.28	5.93	0.30	0.00	0.04	99.24	2.64	52.15	45.21
G5		56.84	0.00	25.17	0.15	0.01	0.01	9.59	6.78	0.31	0.01	0.00	98.87	2.61	57.05	40.34
G5		56.59	0.04	25.99	0.19	0.00	0.00	8.93	6.81	0.45	0.00	0.00	99.00	3.84	58.08	38.08
G5		56.77	0.02	26.18	0.19	0.00	0.01	8.84	6.66	0.41	0.00	0.02	99.10	3.57	57.96	38.47
G5		57.64	0.00	25.87	0.16	0.00	0.01	8.56	6.56	0.39	0.01	0.00	99.20	3.47	58.41	38.11
G5		62.24	0.03	25.02	0.20	0.00	0.00	5.84	6.92	0.42	0.00	0.01	100.68	4.09	67.45	28.46
G6	Core to rim	56.02	0.01	28.40	0.32	0.00	0.06	9.94	4.63	0.24	0.00	0.05	99.67	2.44	47.05	50.51
G6		57.17	0.02	28.34	0.30	0.00	0.07	9.38	5.01	0.28	0.02	0.01	100.60	2.81	50.20	46.99
G6		58.56	0.00	27.35	0.34	0.00	0.05	8.57	5.61	0.32	0.00	0.03	100.83	3.13	54.92	41.95
G6		58.41	0.00	27.47	0.26	0.00	0.12	8.46	5.83	0.37	0.00	0.00	100.92	3.55	55.90	40.56
G6		62.50	0.00	24.86	0.18	0.00	0.04	5.63	6.81	0.56	0.00	0.02	100.60	5.50	66.86	27.64
G6		63.42	0.01	24.17	0.18	0.00	0.08	4.86	7.58	0.47	0.02	0.00	100.79	4.48	72.33	23.19
G7	Core to rim	56.81	0.01	28.14	0.32	0.00	0.18	9.50	4.92	0.26	0.00	0.00	100.14	2.62	49.55	47.83
G7		58.20	0.01	27.29	0.31	0.00	0.11	8.90	5.43	0.31	0.02	0.04	100.62	3.04	53.29	43.67
G7		57.61	0.00	28.18	0.30	0.01	0.04	9.26	5.13	0.32	0.01	0.00	100.86	3.84	58.08	38.08
G7		57.43	0.00	28.16	0.29	0.00	0.05	9.30	5.19	0.30	0.01	0.00	100.73	2.64	52.15	45.21
G7		56.21	0.03	28.76	0.35	0.00	0.12	9.93	4.95	0.26	0.00	0.01	100.62	3.47	58.41	38.11
G8	Core to rim	57.82	0.02	27.63	0.21	0.00	0.05	9.63	4.95	0.26	0.00	0.02	100.59	2.68	47.37	49.95
G8		58.27	0.01	27.12	0.25	0.00	0.01	10.02	5.09	0.29	0.00	0.00	101.06	3.13	52.52	44.35
G8		59.70	0.00	26.82	0.20	0.00	0.14	7.71	5.94	0.30	0.01	0.00	100.82	8.20	27.84	63.96
G8		60.96	0.01	26.23	0.20	0.00	0.01	8.02	5.17	0.34	0.00	0.00	100.94	2.84	46.93	50.23
G8		57.19	0.04	27.42	0.22	0.02	0.00	9.76	5.09	0.30	0.00	0.02	100.06	2.68	48.51	48.82
G8		58.52	0.00	26.53	0.27	0.00	0.02	9.47	4.85	0.37	0.00	0.00	100.03	2.96	50.27	46.77
G8		59.42	0.01	25.35	0.17	0.00	0.00	7.54	6.81	0.52	0.00	0.05	99.87	3.02	60.17	36.81
G8		57.21	0.02	26.84	0.19	0.01	0.00	9.33	6.78	0.36	0.02	0.01	100.77	1.95	55.70	42.36
G8		57.65	0.01	26.05	0.17	0.01	0.00	8.65	6.86	0.46	0.00	0.00	99.86	2.53	57.44	40.02
G8		56.28	0.03	26.23	0.20	0.01	0.00	9.12	7.67	0.35	0.00	0.02	99.91	1.78	59.27	38.95
G8		58.09	0.03	26.05	0.17	0.00	0.00	8.34	7.49	0.33	0.00	0.01	100.51	1.76	60.82	37.42
G8		59.42	0.00	25.59	0.17	0.00	-0.01	7.70	7.78	0.40	0.02	0.01	101.08	2.14	63.26	34.60
G8		59.69	0.01	26.23	0.26	0.00	0.01	8.78	4.71	0.39	0.02	0.02	100.12	4.48	63.17	32.35

granodiorite (An_{23-64}). Geochemically, they can be classified as predominantly andesine and to a lesser degree oligoclase and labradorite. EPMA profiles of An content *vs*. distance (Fig. 7 indicates both oscillatory and normal

Table 4 Major (wt%), trace and rare earth element (ppm) data of representative rock samples from the Ghahan and Sarbadan granitoids

Rock type	Granodiorite			Diorite		
Sample	S1	S2	S3	G1	G2	G3
SiO_2	66.06	66.24	65.60	62.55	55.02	61.79
TiO_2	0.45	0.43	0.57	0.57	0.71	0.58
Al_2O_3	15.87	15.55	15.81	16.73	18.75	16.33
Fe_2O_3	3.79	4.17	5.13	5.63	4.60	5.81
MnO	0.04	0.06	0.14	0.10	0.10	0.09
MgO	1.55	1.71	2.94	2.21	4.01	2.31
CaO	4.86	4.18	5.22	5.67	8.91	5.65
Na_2O	4.31	3.77	2.86	3.54	3.38	3.62
K_2O	2.00	2.44	1.57	1.82	0.57	2.23
P_2O_5	0.09	0.09	0.08	0.12	0.12	0.12
LoI	0.32	0.65	0.57	1.43	1.12	1.35
Total	99.34	99.27	100.49	100.37	97.29	99.89
Cs	0.55	0.48	0.60	0.50	1.59	0.18
Rb	33.00	39.45	42.68	63.21	60.11	19.11
Ba	550.04	691.66	666.43	600.00	470.59	409.89
Th	10.90	9.05	9.06	4.31	5.25	3.94
U	2.74	2.77	2.74	1.53	1.51	1.29
Nb	5.38	4.97	5.02	4.50	5.74	2.86
Ta	0.60	0.57	0.62	0.64	0.55	0.18
K	16596.72	20232.68	13064.20	15108.92	4695.21	18536.78
La	11.96	14.71	12.77	13.00	24.24	6.05
Ce	20.09	25.37	22.68	32.00	44.41	12.86
Pb	4.06	6.87	6.62	5.00	7.34	3.75
Sr	356.03	327.24	304.40	308.50	253.15	410.77
P	373.36	384.87	345.02	530.89	503.62	535.85
Nd	8.48	10.44	9.91	12.00	17.25	8.25
Hf	3.29	3.22	3.58	1.95	3.14	1.72
Zr	132.81	132.28	151.30	59.00	120.59	64.51
Sm	2.00	2.24	2.25	2.34	3.33	2.42
Ti	2687.55	2592.33	3422.09	3437.13	4245.96	3459.07
Tb	0.31	0.34	0.33	0.61	0.48	0.45
Y	12.09	13.13	13.10	12.90	17.40	17.04
Er	1.25	1.36	1.31	1.45	1.47	1.84
Tm	0.19	0.20	0.21	0.19	0.25	0.27
Yb	1.37	1.45	1.47	1.80	1.73	1.79
Co	34.62	43.23	44.50	13.80	33.90	10.13
Cr	9.62	10.81	9.91	9.00	24.39	21.69
Cu	6.94	6.15	19.35	7.00	6.73	1.87
Dy	1.89	2.02	2.03	3.10	2.58	2.90
Mo	0.33	0.44	0.54	0.40	0.80	0.51
Ni	9.45	9.36	10.05	2.00	64.10	22.00
Sc	8.40	8.56	8.32	63.60	11.41	20.22
V	82.35	83.11	74.74	110.00	108.61	175.30
Zn	10.92	69.44	12.21	83.00	40.84	58.87
Ga	13.61	13.65	13.43	19.01	16.24	16.39
As	20.25	-0.20	-0.17	9.70	0.49	4.75
Sn	0.88	0.68	0.58	1.00	0.90	0.52
Sb	1.73	0.16	0.12	0.45	0.90	1.23
Pr	2.24	2.81	2.59	2.99	4.79	1.81
Eu	0.71	0.83	0.78	0.83	0.91	0.76
Gd	1.97	2.30	2.19	1.95	3.22	2.65
Ho	0.43	0.46	0.47	0.61	0.61	0.63
Lu	0.23	0.24	0.24	0.23	0.26	0.28

zoning). Some samples demonstrate high An variations, with the maximum difference in X_{An} in Tafresh plagioclase being more than 30 mol%.

4.3 Crystal Size Distribution (CSD)

4.3.1 3D shape

Table 5 presents the distribution of 2D length and width (intersection dimensions) data of 3,191 measured grains, and Table 6 contains calculated crystal shape data. The two-dimensional size average of plagioclase in the Tafresh granitoids is 0.45 millimeters. Crystal shapes are defined in terms of 'aspect ratio', that is, the ratio of short: intermediate: long (S:I:L) dimensions. Fig. 8 shows frequency *vs.* 2D sa/la (short axis/long axis) histograms, together with the best-fit shape output by CSDSlice5 Spreadsheet (Morgan & Jerram 2006), which compares the distribution of 2D size measurements to a database of shape curves for random sections through different crystal shapes and determines a best fit 3D crystal habit based on regression calculations and fit to the database. Dotted lines show the most similar crystal shapes to our data, and have been considered to be similar to our sample crystal factors

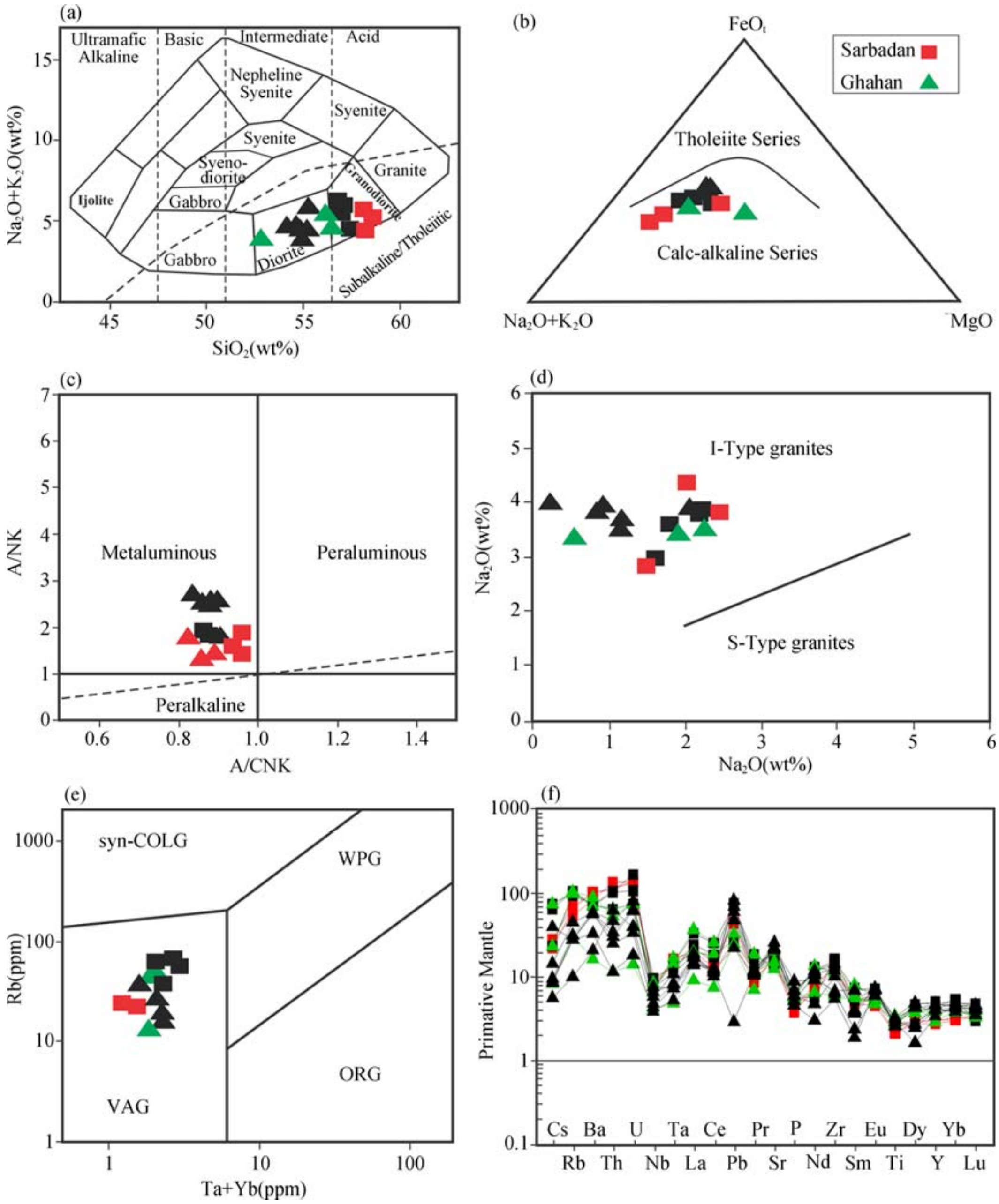

Fig. 5. Chemical classification of rocks from the Ghahan and Sarbadan stocks.

(a) SiO_2 *vs.* K_2O+Na_2O plot (Middlemost, 1994), composition of studied samples range from diorite (Ghahan stock) to granodiorite (Sarbadan stock); (b) AFM (A=Na_2O+K_2O, F=FeOt, M=MgO) diagram with differentiation lines of Irvine and Barager (1971), showing a calc-alkaline affinity for the granitoids; (c) classification of the Ghahan and Sarbadan stocks in A/CNK *vs.* A/NK diagram [ANK=molar $Al_2O_3/(Na_2O+K_2O)$ and ACNK=molar $Al_2O_3/(CaO+Na_2O+K_2O)$], (Shand, 1943); (d) K_2O *vs.* Na_2O classification diagram for discrimination of I- and S-type granitoids (Chappell and White, 2001), all samples fall in the field of I-type granitoids; (e) tectonic classification diagrams (Ta+Yb) *vs.* Rb (Pearce et al. 1984). WPG: within-plate granites; VAG: volcanic arc granites; syn-COLG: syn-collision granites; ORG: oceanic ridge granites; (f) primitive mantle normalized multi-element diagram. Normalizing values are after (McDonough and Sun, 1995). The dark triangle (Ghahan samples) and dark squares (Sarbadan samples) are from Mirnejad et al. (2018).

(Fig. 8). The I/L *vs*. S/I diagram of Zingg (1935) is used here to present the data and to evaluate the three-dimensional (3D) shapes (Fig. 9). In this figure, the plagioclase crystals occur as prolate to bladed in 3D shape.

4.3.2 Residence time of solidification

The CSD curves for plagioclase from Tafresh granitoids are presented in Fig. 10. Most CSD curves do not follow a classic straight line trend. Slopes of CSD curves for Tafresh plagioclase (Fig. 10) become the basis for calculating an average crystal residence time by employing the equation:

$$Tr = (-1/G\times m)/31536000$$

These regression lines are drawn based on all the size intervals, and since the relatively small crystals are more

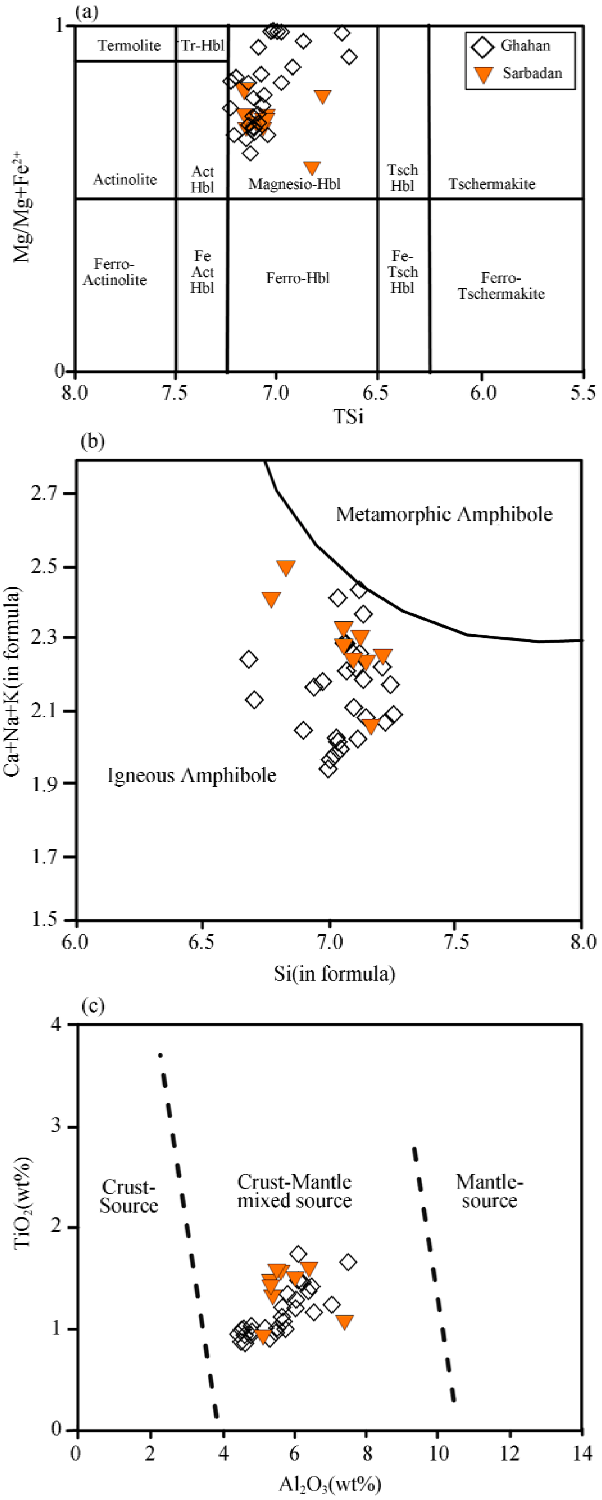

Fig. 6. (a) Diagrams showing the classification of hornblendes according to the nomenclature of Leake et al. (1997); (b) in the (Na+Ca+K) *vs.* Si, all data fall decisively in the igneous field; (c) Plot of TiO_2 *vs.* Al_2O_3 for hornblende, all hornblende crystals fall in the crust-mantle mixed source field (Jiang and An, 1984).

frequent, these lines mostly follow the segments of CSD curves which are related to these crystals. Cashman (1993) noted an important relationship between the cooling rate, and correspondingly, the crystallization rate, with the rate of the plagioclase crystal growth. For example, for a cooling interval of 3 years, which might pertain to a dike, the crystal growth rate is 10^{-9} mm/s, whereas for a cooling interval of 300 years, the growth rate is only one order of magnitude different (10^{-10} mm/s). Investigations by Garrido et al. (2001) and Cheng (2013) of igneous bodies emplaced in the shallow crust similarly indicate a growth rate of ~10^{-10} mm. Cashman (1993) suggested a residence period of less than 1,000 years for the final ascent of shallow intrusive bodies' chambers near the surface and related to the final stages of magma, such as those in the Tafresh granitoids. The crystal residence times of plagioclase from Tafresh are calculated to be less than 1,000 years (Table 6).

Table 5 The estimated dimension of short (x), medium (y) and length (z) axis in CSDSlice environment of plagioclase for the the Ghahan and Sarbadan granitoids

Sample	Counts	3D Shape		
		Short	Intermediate	Long
G1	332	1	1.9	2.8
G2	424	1	1.3	2.3
G3	531	1	1.4	2.5
G4	339	1	1.8	3.2
G5	354	1	1.9	2.5
G6	473	1	1.5	2.2
G7	373	1	1.4	2.6
G8	365	1	1.4	2.5
Total	3191	1	1.7	2.5

Table 6 Line slope, primary nucleation density, and calculated of plagioclase crystallization from the Ghahan and Sarbadan granitoids

Sample	m= regression slope	n_0= regression intercept	Tr= (-1/G×m)/31536000
G1	-1.07	-0.41	339.29
G2	-1.31	0.35	415.40
G3	-1.9	1.92	602.49
G4	-1.32	0.6	418.57
G5	-1.71	1.16	542.24
G6	-2.06	1.74	653.22
G7	-1.2	-0.09	380.52
G8	-1.12	-0.26	355.15
Total	-1.46	1.82	462.96

5 Discussion

5.1 Petrogenesis

As mentioned, Sarbadan and Ghahan granitoids exhibit Nb–Ta–Ti depletion (Fig. 5f), and relative enrichment in Ba, Th, Rb, U, Pb, and K. High Rb, Th, and K, and low Sr, P, and Ti values are diagnostic of typical crustal melts (Harris et al., 1986; Chappell White et al., 2001), suggesting some continental crustal involvement in development of the igneous province. Either interaction occurred between crustal materials or mafic magmas during ascent, or the magma came from an already-enriched mantle source. The common occurrence of magnetite and hornblende in Tafresh indicates a high oxidation state and elevated water content of the parent

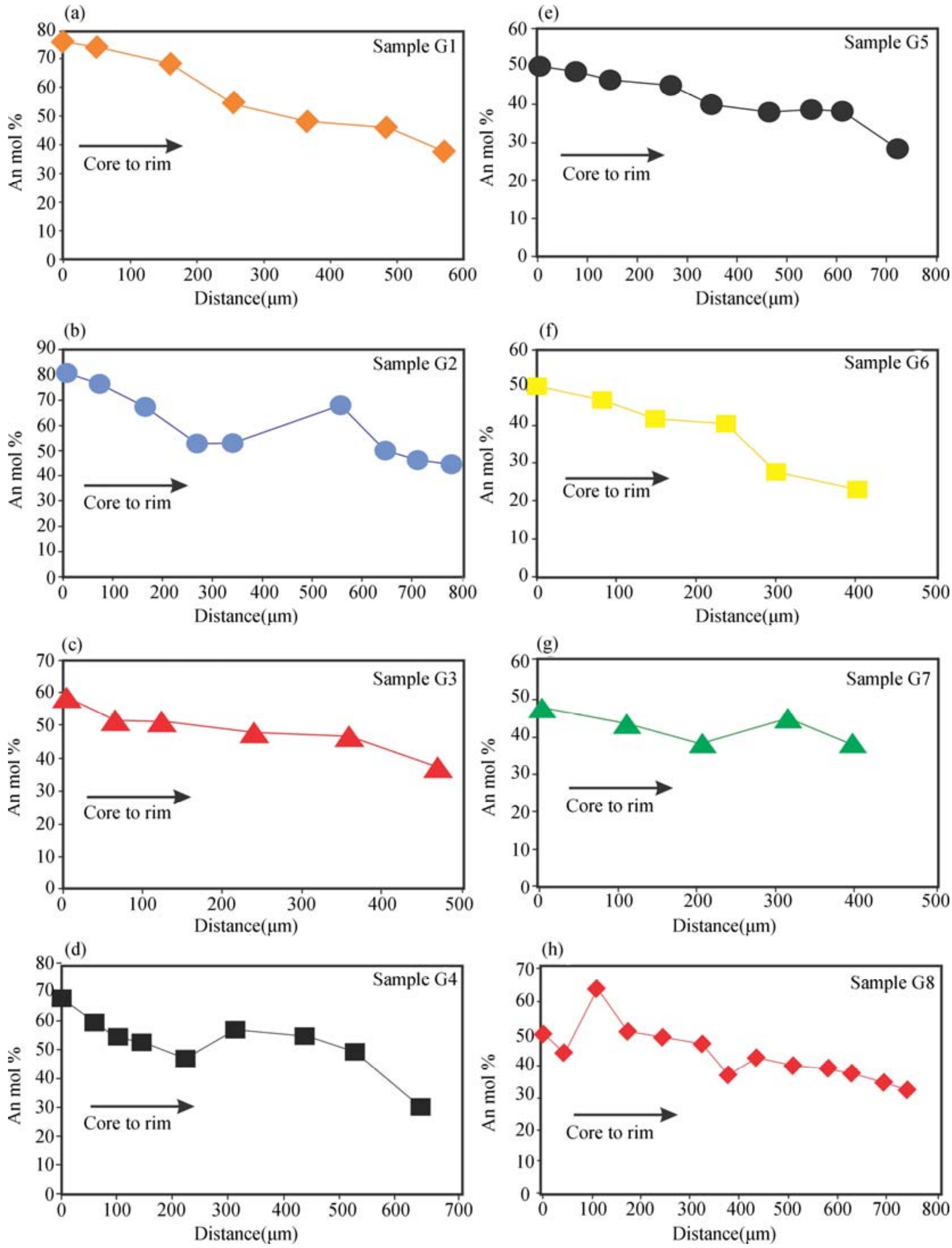

Fig. 7. Measured EMPA profiles for the analyzed plagioclase phenocrysts of the Ghahan granitoids (Samples G1 to G8).

magmas (Hanson, 1980; Saunders et al., 1980), and likely explains the lack of a distinct Eu negative anomaly. In general, the Nb-Ta trough is considered to be a typical characteristic of arc-related I-type granitoids (e.g. Rogers and Hawkesworth, 1989; Sajona et al., 1996). Variations in the enrichment of LREE could be attributed either to varying source compositions or to the amount of partial melting (Langmuir et al., 1977; Le Roex et al., 1987; 1989; Natland, 1989; Niu et al., 1996, 1999; Kamenetsky et al., 2000). On the tectonic discrimination diagram of Pearce et al., (1984), all sample compositions fall in the field of volcanic arc granitoids (Fig. 5e). High Rb, Th, K and low Sr, P and Ti values are compatible with typical crustal melts (Harris et al., 1986; Chappell and White, 1992) and suggest some upper crustal contamination during magmatic evolution.

High LREE and slightly concave-upward pattern MREE to HREE (Fig. 5f) can also reflect amphibole fractionation.

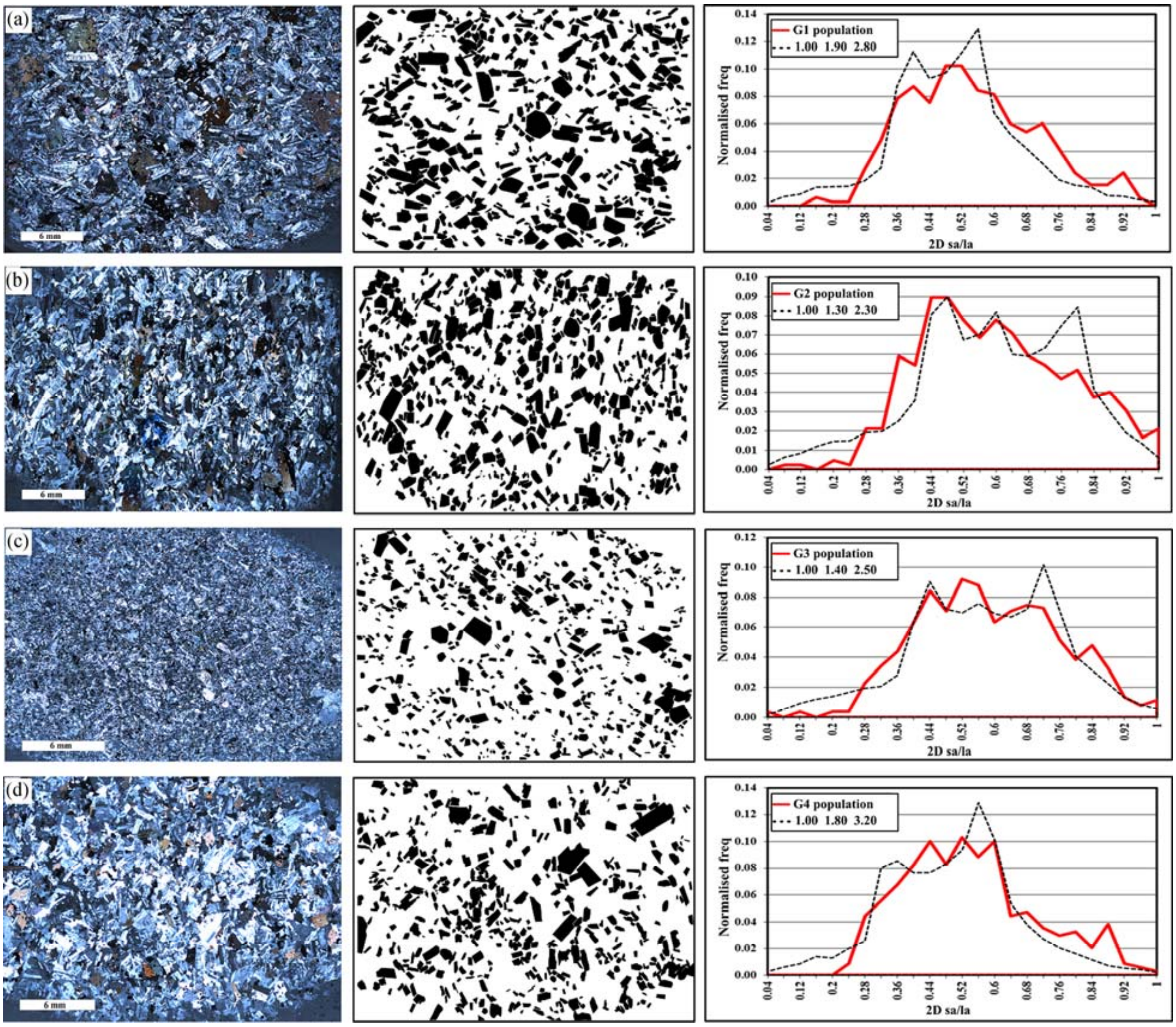

Fig. 8. (a–d) The processed rock sample in the Ghahan granitoids (Sample G1 to G4); (e–h) the processed rock sample in Sarbadan granitoids (Sample G5 to G8). Mosaic thin sections, binary images and two dimensional width/length distributions for each sample (red line) are shown along with their best fit crystal habit (dashed lines) as determined by CSDSlice (Morgan and Jerram, 2006). The numbers on the left corner of the CSDSlice diagram represent the aspect ratios as given by short axis: intermediate axis: long axis of the crystal. The outlines are plagioclase.

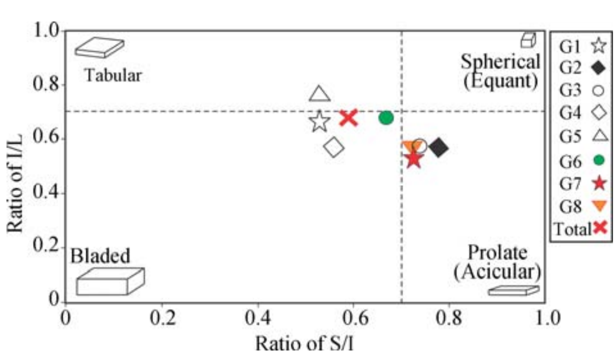

Fig. 9. The position of the average aspect ratio of plagioclase in granitoid rocks on the I/L *vs.* S/I diagram (Zingg, 1935). S, I and L represent small, intermediate and long axis, respectively.

Amphibole typically has a high distribution constant (KD) for Nb. The geochemical characteristics of the studied samples strongly suggest that rather high pressure fractional crystallization (involving amphibole but not garnet) is responsible here for the generation of this rock type. If garnet, which sequesters HREEs, had been involved in magma fractionation, abundances of HREEs would have been far lower than the observed abundances (Fujimaki et al., 1984). This indicates that Tafresh magma was not separated from a source melt in which garnet had been restite. Substantial amounts of garnet were not involved, whether as residue during partial melting, or during fractionation or final re-equilibration of the magma. The magmas were produced in a T-P-XH_2O environment outside the garnet stability field, possibly in an amphibole-bearing mantle source.

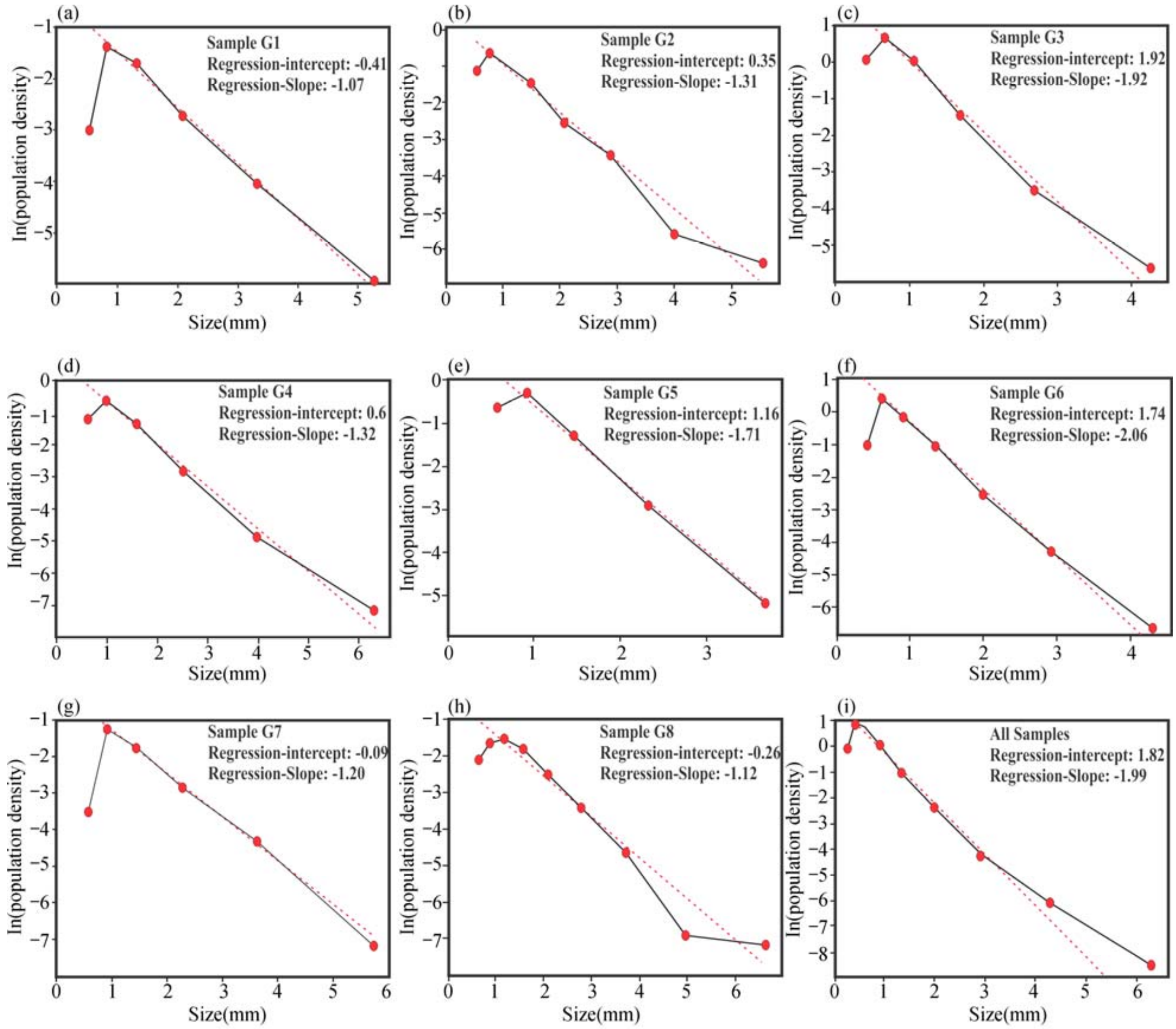

Fig. 10. (a–i) CSD diagrams of the studied plagioclase crystals from Tafresh granitoids. Note the non-linear trend of the diagrams (especially in figs. b, h and i). The dotted lines are the regression lines calculated based on the frequency of crystal sizes, the horizontal axis unit is the millimeter.

5.2 Pressure and temperature conditions of crystallization

Aluminum-in-hornblende barometry has been widely used in calc-alkaline granitoids to calculate pressures of magmatic crystallization and corresponding emplacement depths (e.g., Hammarstrom and Zen, 1986; Hollister et al., 1987; Anderson and Smith, 1995; Stein and Dietl, 2001; Ernst, 2002), implying the computed pressure can be attributed to the crystallization of hornblende, and not necessarily to the consolidation of the bulk granitic rock (Ague, 1997). The theory of Al-hornblende barometry requires a buffer assemblage (quartz + plagioclase + alkali feldspar + biotite + hornblende + titanite + magnetite or ilmenite), which limits the applicability of the method (Leake and Said, 1994; Ague, 1997). It is standard practice to analyze Al in hornblende crystal rims, thus to represent the final (near-solidus) conditions of the magma. We have chosen the calibration of Schmidt (1992) as being more reliable than the other methods for considering the influence of temperature and oxygen fugacity on the pressure calculation (Stein and Dietl, 2001; Toummite et al., 2012). The Al-in-hornblende barometry of Schmidt (1992) is applied to calculate pressure and temperature (P (±0:6 kbar)=−3:01 + 4:76 Altot, r^2=0:99). In general, the lower Altot contents in the amphiboles of Tafresh granodiorites (with mean 0.95) are indicative of a low pressure of crystallization. Table 7 summarizes the results of crystallization pressures calculated from hornblende composition. Also, we used the Al^{iv}+Al^{vi} *vs.* Fe/(Fe+Mg) diagram of Anderson and Smith (1995) for determination of the amphibole crystallization pressure. It suggests that the amphiboles crystallized under pressures of about 3 kbar (Fig. 11a). Furthermore, in the diagram of Al_{tot} *vs* P (kbar) (Anderson and Smith, 1995), all of the samples indicate a crystallization temperature of less than 750°C (Fig. 11b) that are consistent with the calculated temperatures and pressures (Table 7).

5.3 Estimation of oxygen fugacity (fO_2)

Oxygen fugacity (or oxygen potential) is a powerful mechanism for understanding the crystallization of igneous and metamorphic rocks under variable pressure, temperature, and melt composition conditions (Toummite et al., 2012). The intrinsic oxygen fugacity of a magma is related to its source material, which in turn is related to the tectonic setting. More highly oxidized magmas are commonly associated with convergent plate boundaries (Ewart, 1979), whereas felsic magmas formed by fractionation from mantle-derived magmas in rift zones are more reduced (Loiselle, 1979). Ridolfi et al. (2010) proposed an empirical universal amphibole sensor to estimate fO_2, which, when applied to data for the Ghahan and Sarbadan rocks, provided calculated values of log fO_2 in the range of −10.1 to −13.3 (with a mean −12.52).

5.4 Magmatic processes

As noted, a CSD diagram is a quantitative description of relationships between crystal size and crystal population density (Cashman and Marsh, 1988; Higgins, 2000; 2002; 1998; 1994; 1996; Marsh, 1998; 1988). These diagrams show changes in frequency and crystal sizes as a function of the latent residency time in the system. A linear CSD diagram indicates simple, monotonic cooling of magma, but if the diagram exhibits kinks, or changes of slope (Fig. 10B, C, H and I), additional processes must have been superimposed upon the cooling. One possibility is coarsening, whereby small crystals are consumed by annealing as large crystals grow larger (Fig. 12d). Another possibility is the mixing of populations of crystals that had formed in different sources during rapid ascent or magma mixing (Fig. 12e).

It is noteworthy that the Tafresh granitoids contain abundant globular or elliptical MMEs of various sizes, since the existence of MMEs in the Tafresh granitoids provides an insight into the dynamics of the magma chambers. They are characterized by a fine-grained microgranular texture and are structurally massive with chilled margins towards the MME rims. Darker and finer chilled margins are products of the interaction between felsic host rocks and their mafic magmatic enclaves (e.g., Bussy, 1991; Didier and Barbarin, 1991). MMEs could be restites (Chappell et al., 1987; Chappell and Stephens, 1988; Chen et al., 1998), or they could be inclusions of mantle-derived mafic magma (Eichelberger, 1980; Vernon, 1984; Holden et al., 1987; Bonin, 2004; Yang et al., 2006), remnants of lower crustal mafic rocks (Kepezhinskas et al. 1997; Maas et al. 1997), or products

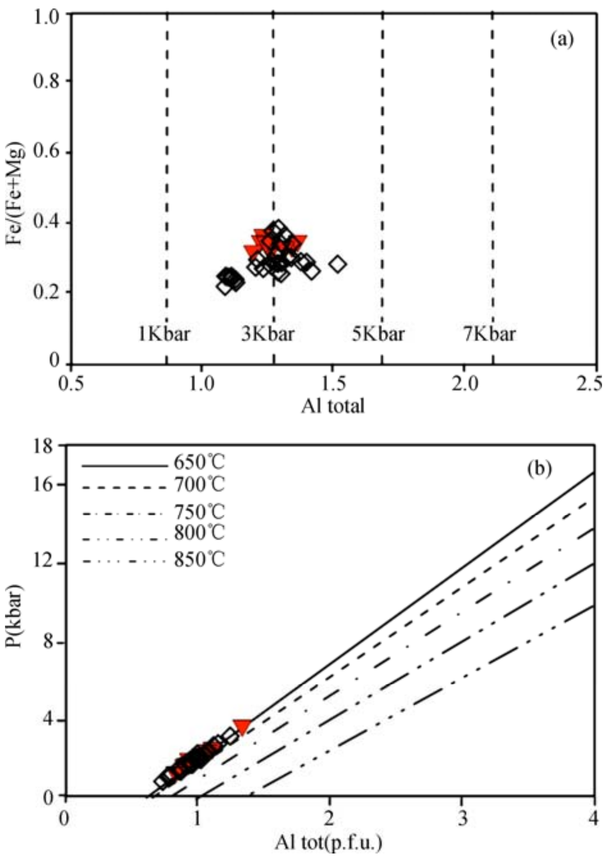

Fig. 11. (a) The position of the Tafresh granitoids on a $Al^{iv}+Al^{vi}$ *vs.* Fe/(Fe+Mg) diagram (Anderson and Smit, 1995); (b) determination of the amphibole crystallization pressure, Al (t) *vs.* P (kbar) diagram (Anderson and Smit, 1995) suggests that the amphiboles crystallized under pressures of about 3 kbar.

Table 7 Crystallization pressure calculated of amphiboles from the Ghahan and Sarbadan granitoids (in kbar).

	Sample	Hammarstrom & Zen 86	Johnson & Rutherford 89	Schmidt 92	Anderson & Smith	Continental depth (km)
Ghahan	Gh1	1.4	1.0	2.0	2.0	3.3
	Gh2	1.5	1.1	2.1	2.1	3.4
	Gh3	1.4	1.0	2.0	2.0	3.3
	Gh4	0.9	0.6	1.5	1.5	2.8
	Gh5	1.0	0.7	1.7	1.7	3.0
	Gh6	1.3	0.9	1.9	1.9	3.2
	Gh7	1.0	0.7	1.7	1.7	3.0
	Gh8	0.5	0.3	1.2	1.2	2.6
	Gh9	-0.1	-0.2	0.6	0.6	2.2
	Gh10	-0.1	-0.3	0.6	0.6	2.1
	Gh11	2.3	1.8	2.9	2.8	4.3
	Gh12	1.9	1.4	2.5	2.4	*
	Gh13	-0.2	-0.3	0.5	0.5	*
	Gh14	0.8	0.5	1.5	1.4	2.8
	Gh15	0.0	-0.2	0.7	0.7	*
	Gh16	-0.1	-0.2	0.6	0.6	*
	Gh17	-0.2	-0.4	0.5	0.5	*
	Gh18	1.1	0.8	1.8	1.7	3.1
	Gh19	0.0	-0.1	0.7	0.7	*
	Gh20	1.1	0.7	1.7	1.7	*
	Gh21	1.1	0.8	1.8	1.7	*
	Gh22	0.9	0.6	1.5	1.5	2.9
	Gh23	1.1	0.7	1.7	1.7	3.0
	Gh24	0.8	0.5	1.4	1.4	2.8
	Gh25	1.0	0.6	1.6	1.6	2.9
	Gh26	1.7	1.3	2.3	2.3	3.6
	Gh27	0.5	0.3	1.2	1.2	2.6
Sarbadan	Sa1	0.7	0.4	1.4	1.3	2.7
	Sa2	0.7	0.4	1.4	1.4	2.7
	Sa3	1.5	1.1	2.1	2.1	3.4
	Sa4	1.2	0.9	1.9	1.9	3.2
	Sa5	2.8	2.2	3.3	3.3	*
	Sa6	0.7	0.4	1.4	1.4	2.7
	Sa7	0.7	0.4	1.4	1.4	2.7
	Sa8	0.9	0.6	1.5	1.5	2.8
	Sa9	0.4	0.2	1.1	1.1	2.5

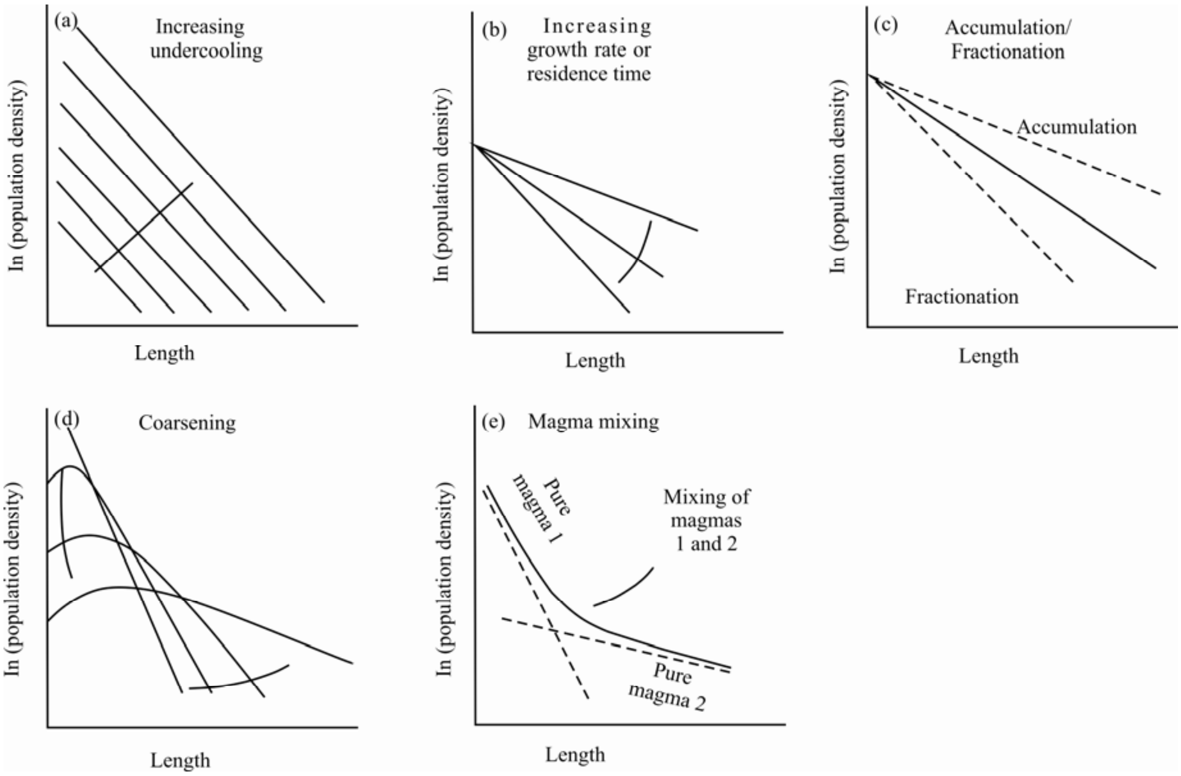

Fig. 12. Schematic examples of processes that can influence the shape of the CSD (after Higgins, 2006, modified by Vinet & Higgins 2010).

(a) Increase of the cooling rate; (b) decrease in line slope resulting in an increasing in growth and residency time in the magma chamber; (c) different segregation effects or crystal accumulations in the system; (d) effects of the presence of coarse grains on the CSD diagram; (e) mixing of two magmas with different crystal densities or coarse-grained crystals. Each of these processes can have an effect on CSD through changing some characteristics, such as residency time.

of magma mixing (e.g. Didier and Barbarin, 1991; Perugini et al., 2003). MMEs are identified here on the basis of their dark color, grain size and textural properties. K-feldspar and plagioclase megacrysts in the MMEs (Fig. 4), together with the presence of feldspars and quartz that were entrained from the host granitoids to the MMEs, suggest a hybrid system formed by the mixing of two distinct end-member magma compositions (e.g., Barbarin, 1990; Hibbard, 1991; Yang et al., 2015). Additionally, the presence of acicular apatite in the MMEs suggests that the mafic magma was injected into the felsic magma, and crystallization in a quenched environment occurred as a result of the mingling of small volumes of hot mafic melt with cooler granitoid magma (e.g., Vernon, 1984; Chen et al., 2009, 2016). Another notable point for magma mixing can be zoning in plagioclase, which is expressed as An% content, and can be governed by a number of factors, among which are changes in temperature, water fugacity (e.g. Loomis and Welber, 1982; Pietranik and Koepke, 2014), and magma composition associated with recharging by more mafic magma (e.g. Tepley et al., 1999; Ginibre et al., 2002; Browne et al., 2006; Nicotra and Viccaro, 2012).

As already noted, the maximum difference in X_{An} in Tafresh plagioclase is more than 30 mol%. Variations in An content, which can be very large and abrupt, are due to fractionation, and/or the differences in sources, assimilation of wall rocks, and other magmatic processes (see Yang and Lentz, 2005) and variation in the crystallization condition. Ghiorso et al. (1983) showed that if temperature varies by 10°C, the X_{An} value would change by 1 mol%. Therefore, the sample would require an unreasonably high change in temperature of 300°C if temperature alone had caused the variation in X_{An}. Ghiorso et al. (1983) further showed that if pressure varied by 1 kbar then the An value would change by 1.4 mol%. Longhi et al. (1993) specified that a 1 kbar increase in pressure, acting alone, leads to a 1 mol% decrease in X_{An}. Similarly, the 30 mol% range in X_{An} would correspond to an absurdly large pressure range of about 30 kbar. It is more plausible that a process of magma mixing has been responsible in this instance.

Finally, and as a result, the presence of the sieve texture, microgranular enclaves, oscillatory zoning in plagioclase crystals and the changes in the slope of the CSD line together indicate the possibility of magma mixing in the Tafresh granitoids. Generally, magma mixing has been shown to have a large influence on the mineralogical, textural and geochemical conditions of arc-related rocks (Tepley et al., 1999).

6 Conclusions

The Tafresh granitoids, which are part of the Urumieh-Dokhtar Magmatic Arc in central Iran, are I-type, metaluminous, and calc-alkaline.

The chemical compositions of the amphiboles, which are calc-alkaline, indicate a high oxygen fugacity, which is consistent with a mixed crust-mantle magma source. On the basis of Altot contents in the amphiboles of Tafresh granodiorites, the final crystallization is indicative of a low pressure of crystallization.

Calculated residence times for Tafresh plagioclase crystals is less than 1,000 years, which supports field evidence that these plutons were emplaced at shallow depths. The shape of the CSD curves in the samples are consistent with the standard magma mixing CSD patterns.

The presence of sieve texture, microgranular enclaves (MMEs), oscillatory zoning in plagioclase crystals and variations in the slopes of CSD lines are a consequence of magma mixing in the Tafresh granitoids.

Acknowledgements

Dear Prof. Leon E Long kindly reviewed an earlier version of this manuscript. We thank Hamed Pourkhorsandi for obtaining the mosaic images of the rock samples at the CEREGE institute of Aix-Marseille University (France). We thank the Iranian Mines and Mining Industries Development and Renovation Organization (IMIDRO) for help with the microprobe data. We would also like to thank Prof. Liu Lian for the editorial handling of this paper and two anonymous reviewers for their constructive comments.

Manuscript received Jun. 10, 2018
accepted Mar. 18, 2019
associate EIC HAO Ziguo
edited by Jeff LISTON and FEI Hongcai

References

Agard, P., Omrani, J., Jolivet, L., Whitechurch, H., Vrielynck, B., Spakman, W., and Wortel, R., 2011. Zagros orogeny: a subduction-dominated process. Geological Magazine, 148(5–6) : 692–725.

Ague, J. J., 1997. Thermodynamic calculation of emplacement pressures for batholithic rocks, California: Implications for the aluminum-in-hornblende barometer. Geology, 25(6): 563–566.

Alavi, M., 1994. Tectonics of the Zagros orogenic belt of Iran: new data and interpretations. Tectonophysics, 229(3-4), 211-238.

Alavi, M., 2004. Regional stratigraphy of the Zagros fold-thrust belt of Iran and its proforeland evolution. American Journal of Science, 304(1): 1 –20.

Anderson, J.L., and Smith, D.R., 1995. The effects of temperature and fO_2 on the Al-in-hornblende barometer. American Mineralogist, 80(5–6) : 549–559.

Barbarin, B., 1990. Plagioclase xenocrysts and mafic magmatic enclaves in some granitoids of the Sierra Nevada batholith, California. Journal of Geophysical Research, 95: 17747 – 17756.

Baxter, S., and Feely, M., 2002. Magma mixing and mingling textures in granitoids: examples from the Galway Granite, Connemara, Ireland. Mineralogy and Petrology, 76: 63–74.

Berberian, F., and Berberian, M., 1981. Tectono‑plutonic episodes in Iran. Zagros Hindu Kush Himalaya Geodynamic Evolution, 5–32.

Berberian, F., Muir, I.D., Pankhurst, R.J., and Berberian, M., 1982. Late Cretaceous and early Miocene Andean-type plutonic activity in northern Makran and Central Iran. Journal of the Geological Society, 139(5): 605–614.

Bonin, B., 2004. Do coeval mafic and felsic magmas in post-collisional to within-plate regimes necessarily imply two contrasting, mantle and crustal, sources? A review. Lithos, 78 (1–2) : 1 –24.

Browne, B.L., Eichelberger, J.C., Patino, L.C., Vogel, T.A., Uto, K., and Hoshizumi, H., 2006. Magma mingling as indicated by texture and Sr/Ba ratios of plagioclase phenocrysts from Unzen volcano, SW Japan. Journal of Volcanology and Geothermal Research, 154(1–2) : 103–116.

Bussy, F., 1991. Enclaves of the late Miocene monte capanne granite, Elba island, Italy. In: Didier, J., and Barbarin, B. (eds.), Enclaves and Granite Petrology. Developments in Petrology, 13. Elsevier, Amsterdam, 167–178.

Cashman, K.V., 1990. Textural constraints on the kinetics of crystallization of igneous rocks. Reviews in Mineralogy and Geochemistry, 24(1): 259–314.

Cashman, K.V., 1993. Relationship between plagioclase crystallization and cooling rate in basaltic melts. Contributions to Mineralogy and Petrology, 113(1): 126–142

Cashman, K.V., and Marsh, B.D., 1988. Crystal size distribution (CSD) in rocks and the kinetics and dynamics of crystallization II: Makaopuhi Lava Lake. Contributions to Mineralogy and Petrology, 99(3): 292–305.

Castro, J.M., Cashman, K.V., and Manga, M., 2004. A technique for measuring 3D crystal-size distributions of prismatic microlites in obsidian. American Mineralogist, 88(8–9): 1230 –1240.

Chappell, B.W. and Stephens, W.E., 1988. Origin of infracrustal (I-type) granite magmas. Transactions of the Royal Society of Edinburgh: Earth Sciences, 79(2–3): 71–86.

Chappell, B.W., and White, A.J.R., 1992. I-and S-type granites in the Lachlan Fold Belt. Transactions of the Royal Society of Edinburgh: Earth Sciences, 83(1–2): 1–26.

Chappell, B.W., and White, A.J., 2001. Two contrasting granite types: 25 years later. Australian Journal of Earth Sciences, 48 (4): 489–499.

Chappell, B.W., White, A.J.R., and Wyborn, D., 1987. The importance of residual source material (restite) in granite petrogenesis. Journal of Petrology, 28(6): 1111–1138.

Chen, B., Chen, Z.C., and Jahn, B.M., 2009. Origin of the mafic enclaves from the Taihang Mesozoic orogen, north China craton. Lithos, 110: 343–358.

Chen, C.J., Chen, B., Li, Z., and Wang, Z.Q., 2016. Important role of magma mixing in generating the Mesozoic monzodioriticegranodioritic intrusions related to Cu mineralization, Tongling, East China: evidence from petrological and in situ Sr-Hf isotopic data. Lithos, 248–251: 80–93.

Chen, J., and Jahn, B.M., 1998. Crustal evolution of southeastern China: Nd and Sr isotopic evidence. Tectonophysics, 284(1–2): 101–133.

Didier, J., and Barbarin, B., 1991. Enclaves and Granite Petrology. In: Developments in Petrology, Vol. 13. Elsevier, Amsterdam.

Eichelberger, J.C., 1980. Vesiculation of mafic magma during replenishment of silicic magma reservoirs. Nature, 288(5790): 446.

Ernst, W.G., 2002. Paragenesis and thermobarometry of Ca-amphiboles in the Barcroft granodioritic pluton, central White Mountains, eastern California. American Mineralogist, 87(4): 478–490.

Ewart, A., 1979. A review of the mineralogy and chemistry of Tertiary-Recent dacitic, latitic, rhyolitic, and related salic volcanic rocks. In Developments in Petrology (6: 13–121). Elsevier.

Fialin, M., 1988. Modification of Philibert-Tixier ZAF correction for geological samples. X‑Ray Spectrometry, 17(3): 103-106.

Fujimaki, H., Tatsumoto, M., and Aoki, K.I., 1984. Partition coefficients of Hf, Zr, and REE between phenocrysts and groundmasses. Journal of Geophysical Research: Solid Earth, 89(2): 662–672.

Garrido, C. J., Kelemen, P. B., and Hirth, G., 2001. Variation of cooling rate with depth in lower crust formed at an oceanic spreading ridge: Plagioclase crystal size distributions in gabbros from the Oman ophiolite. Geochemistry, Geophysics, Geosystems, 2(10).

Ghiorso, M. S., Carmichael, I. S., Rivers, M. L., and Sack, R. O., 1983. The Gibbs free energy of mixing of natural silicate liquids; an expanded regular solution approximation for the calculation of magmatic intensive variables. Contributions to Mineralogy and Petrology, 84(2–3): 107–145.

Ginibre, C., Wörner, G., and Kronz, A., 2002. Minor-and trace-element zoning in plagioclase: implications for magma chamber processes at Parinacota volcano, northern Chile. Contributions to Mineralogy and Petrology, 143(3): 300–315.

Grogan, S.E., and Reavy, R.J., 2002. Disequilibrium textures in the Leinster granite complex, SE Ireland: evidence for acid-acid magma mixing. Mineralogical Magazine, 66: 929–939.

Hajian, J., 2001. Geology of Tafresh. Geological and Mineralogical Exploration Survey of Iran, Tehran. No. 82. Report.

Hammarstrom, J.M., and Zen, E.A., 1986. Aluminum in hornblende: an empirical igneous geobarometer. American Mineralogist, 71(11–12): 1297–1313.

Hanson, G.N., 1980. Rare earth elements in petrogenetic studies of igneous systems. Annual Review of Earth and Planetary Sciences, 8(1): 371–406.

Harris, N.B., Pearce, J.A., and Tindle, A.G., 1986. Geochemical characteristics of collision-zone magmatism. Geological Society, London, Special Publications, 19(1): 67–81.

Higgins, M.D., 1994. Determination of crystal morphology and size from bulk measurements on thin sections: numerical modelling. American Mineralogist, 79: 113–119.

Higgins, M.D., 1996. Crystal size distributions and other quantitative textural measurements in lavas and tuff from Egmont volcano (Mt. Taranaki), New Zealand. Bulletin of Volcanology, 58(2–3): 194–204.

Higgins, M.D., 1998. Origin of anorthosite by textural coarsening: quantitative measurements of a natural sequence of textural development. Journal of Petrology, 39(7): 1307–1323.

Higgins, M.D., 2000. Measurement of crystal size distributions. American Mineralogist, 85(9): 1105–1116.

Higgins, M.D., 2002. Closure in crystal size distributions (CSD), verification of CSD calculations, and the significance of CSD fans. American Mineralogist, 87(1): 171–175.

Higgins, M.D., 2006. Quantitative textural measurements in igneous and metamorphic petrology. Cambridge University Press.

Higgins, M.D., 2011. Textural coarsening in igneous rocks. International Geology Review, 53(3–4): 354–376.

Holden, P., Halliday, A.N., and Stephens, W.E., 1987. Neodymium and strontium isotope content of microdiorite enclaves points to mantle input to granitoid production. Nature, 330(6143): 53.

Hollister, L.S., Grissom, G.C., Peters, E.K., Stowell, H.H., and Sisson, V.B., 1987. Confirmation of the empirical correlation of Al in hornblende with pressure of solidification of calc-alkaline plutons. American Mineralogist, 72(3–4): 231–239.

Huppert, H.E., Stephen, R., and Sparks, J., 1989. Chilled margins in igneous rocks. Earth and Planetary Science Letters, 92: 397-405.

Irvine, T.N.J., and Baragar, W.R.A.F., 1971. A guide to the chemical classification of the common volcanic rocks. Canadian Journal of Earth Sciences, 8(5): 523–548.

Jerram, D.A., and Cheadle, M.J., 2000. On the cluster analysis of grains and crystals in rocks. American Mineralogist, 85(1): 47–67.

Jerram, D.A., and Higgins, M.D., 2007. 3D analysis of rock textures: quantifying igneous microstructures. Elements, 3(4): 239–245.

Jiang, C.Y., and An, S.Y., 1984. On chemical characteristics of calcic amphiboles from igneous rocks and their petrogenesis significance. Journal of Mineralogy and Petrology, 3: 1–9 (in Chinese with English abstract).

Kamenetsky, V.S., Everard, J.L., Crawford, A.J., Varne, R., Eggins, S.M., and Lanyon, R., 2000. Enriched end-member of primitive MORB melts: petrology and geochemistry of glasses from Macquarie Island (SW Pacific). Journal of Petrology, 41(3): 411–430.

Kepezhinskas, P., McDermott, F., Defant, M.J., Hochstaedter, A., Drummond, M.S., Hawkesworth, C.J., and Bellon, H., 1997. Trace element and Sr Nd- Pb isotopic constraints on a three-component model of Kamchatka Arc petrogenesis. Geochimica et Cosmochimica Acta, 61(3): 577–600.

Kuşcu, G.G., and Floyd, P.A., 2001. Mineral compositional and textural evidence for magma mingling in the Saraykent volcanics. Lithos, 56(2–3): 207–230.

Langmuir, C.H., Bender, J.F., Bence, A.E., Hanson, G.N., and Taylor, S.R., 1977. Petrogenesis of basalts from the FAMOUS area: Mid-Atlantic Ridge. Earth and Planetary Science Letters, 36(1): 133–156.

Le Roex, A.P., Dick, H.J., Gulen, L., Reid, A.M., and Erlank, A.J., 1987. Local and regional heterogeneity in MORB from the Mid-Atlantic Ridge between 54.5 S and 51 S: Evidence for geochemical enrichment. Geochimica et Cosmochimica Acta, 51(3): 541–555.

Leake, B.E., 1997. Nomenclature of Amphiboles. Report of the subcommittee on Amphiboles of the International Mineralogical Association, Commission on new minerals and mineral names. The Canadian Mineralogist, 35: 219–246.

Leake, B.E., and Said, Y.A., 1994. Hornblende barometry of the Galway Batholith, Ireland: an empirical test. Mineralogy and Petrology, 51(2–4): 243–250.

Leake, B.E., Woolley, A.R., Birch, W.D., Burke, E.A., Ferraris, G., Grice, J.D., and Stephenson, N.C., 2004. Nomenclature of amphiboles: additions and revisions to the International Mineralogical Association's amphibole nomenclature. Mineralogical Magazine, 68(1): 209–215.

Loiselle, M.C., 1979. Characteristics and origin of anorogenic granites. In: Geological Society of America Abstracts with Programs (11: 468).

Longhi, J., Fram, M.S., Vander Auwera, J., and Montieth, J.N., 1993. Pressure effects, kinetics, and rheology of anorthositic and related magmas. American Mineralogist, 78(9–10): 1016–1030.

Loomis, T.P., and Welber, P.W., 1982. Crystallization processes in the Rocky Hill granodiorite pluton, California: an interpretation based on compositional zoning of plagioclase. Contributions to Mineralogy and Petrology, 81 (3): 230–239.

Lowell, G.R., and Young, G.J., 1999. Interaction between coeval mafic and felsic melts in the St. Francois Terrane of Missouri, USA. Precambrian Research, 95: 69–88.

Maas, R., Nicholls, I.A., and Legg, C., 1997. Igneous and metamorphic enclaves in the S-type Deddick granodiorite, Lachlan Fold Belt, SE Australia: petrographic, geochemical and Nd-Sr isotopic evidence for crustal melting and magma mixing. Journal of Petrology, 38(7): 815–841.

Marsh, B.D., 1988. Crystal size distribution (CSD) in rocks and the kinetics and dynamics of crystallization. Contributions to Mineralogy and Petrology, 99(3): 277–291.

Marsh, B.D., 1998. On the interpretation of crystal size distributions in magmatic systems. Journal of Petrology, 39 (4): 553–599.

McDonough, W.F., and Sun, S.S., 1995. The composition of the Earth. Chemical Geology, 120(3–4): 223–253.

Middlemost, E.A., 1994. Naming materials in the magma/ igneous rock system. Earth-Science Reviews, 37(3–4): 215–224.

Mock, A., and Jerram, D.A., 2005. Crystal size distributions (CSD) in three dimensions: insights from the 3D reconstruction of a highly porphyritic rhyolite. Journal of Petrology, 46(8): 1525–1541.

Mock, A., Jerram, D.A., and Breitkreuz, C., 2003. Using quantitative textural analysis to understand the emplacement of shallow-level rhyolitic laccoliths—a case study from the Halle Volcanic Complex, Germany. Journal of Petrology, 44 (5): 833–849.

Morgan, D.J., and Jerram, D.A., 2006. On estimating crystal shape for crystal size distribution analysis. Journal of Volcanology and Geothermal Research, 154(1–2): 1–7.

Natland, J.H., 1989. Partial melting of a lithologically heterogeneous mantle: inferences from crystallization histories of magnesian abyssal tholeiites from the Siqueiros Fracture Zone. Geological Society, London, Special Publications, 42(1): 41–70.

Niu, Y., Collerson, K.D., Batiza, R., Wendt, J.I., and Regelous, M., 1999. Origin of enriched‐type mid‐ocean ridge basalt at ridges far from mantle plumes: The East Pacific Rise at 11 20′ N. Journal of Geophysical Research: Solid Earth, 104(B4), 7067–7087.

Niu, Y., Waggoner, D. G., Sinton, J.M., and Mahoney, J.J., 1996. Mantle source heterogeneity and melting processes beneath seafloor spreading centers: the East Pacific Rise, 18–19 S. Journal of Geophysical Research: Solid Earth, 101(B12): 27711–27733.

Pearce, J.A., Harris, N.B., and Tindle, A.G., 1984. Trace element discrimination diagrams for the tectonic interpretation of granitic rocks. Journal of Petrology, 25(4): 956–983.

Perugini, D., Poli, G., Christofides, G., and Eleftheriadis, G., 2003. Magma mixing in the Sithonia Plutonic Complex, Greece: evidence from mafic microgranular enclaves. Mineralogy and Petrology, 78(3–4): 173–200.

Pietranik, A., and Koepke, J., 2014. Plagioclase transfer from a host granodiorite to mafic microgranular enclaves: diverse records of magma mixing. Mineralogy and Petrology, 108(5): 681–694.

Pourkhorsandi, H., Mirnejad, H., Raiesi, D., and Hassanzadeh, J., 2015. Crystal size and shape distribution systematics of plagioclase and the determination of crystal residence times in the micromonzogabbros of Qisir Dagh, SE of Sabalan volcano (NW Iran). Geologica Carpathica, 66(4): 257–268.

Randolph, A.D., and Larson, M.A., 1988. Theory of particulate processes: Analysis and Techniques of Continuous Crystallization (2nd Edition). Academic Press, New York.

Renzulli, A., and Santi, P., 1997. Sub-volcanic crystallization at Stromboli (Aeolian Islands, southern Italy) preceding the Sciara del Fuoco sector collapse: evidence from monzonite lithic suite. Bulletin of Volcanology, 59(1): 10–20.

Ridolfi, F., Renzulli, A., and Puerini, M., 2010. Stability and chemical equilibrium of amphibole in calc-alkaline magmas: an overview, new thermobarometric formulations and application to subduction-related volcanoes. Contributions to Mineralogy and Petrology, 160(1): 45–66.

Rogers, G., and Hawkesworth, C.J., 1989. A geochemical traverse across the North Chilean Andes: evidence for crust generation from the mantle wedge. Earth and Planetary Science Letters, 91(3–4): 271–285.

Sajona, F.G., Maury, R.C., Bellon, H., Cotten, J., and Defant, M., 1996. High Field Strength Element Enrichment of Pliocene—Pleistocene Island Arc Basalts, Zamboanga Peninsula, Western Mindanao (Philippines). Journal of Petrology, 37(3): 693–726.

Sarjoughian, F., Kananian, A., Haschke, M., Ahmadian, J., and Ling, W., 2012. Magma mingling and hybridization in the Kuh-e Dom pluton, Central Iran. Journal of Asian Earth Sciences, 54–55: 49–63.

Saunders, A.D., Tarney, J., and Weaver, S.D., 1980. Transverse geochemical variations across the Antarctic Peninsula: implications for the genesis of calc-alkaline magmas. Earth and Planetary Science Letters, 46(3): 344–360.

Schmidt, M.W., 1992. Amphibole composition in tonalite as a function of pressure: an experimental calibration of the Al-in-hornblende barometer. Contributions to Mineralogy and Petrology, 110(2–3) : 304–310.

Shand, S.J., 1943. Eruptive rocks: their genesis, composition, and classification, with a chapter on meteorites.

Stein, E., and Dietl, C., 2001. Hornblende thermobarometry of granitoids from the Central Odenwald (Germany) and their implications for the geotectonic development of the Odenwald. Mineralogy and Petrology, 72(1–3): 185–207.

Tepley, F.J., Davidson, J.P., and Clynne, M.A., 1999. Magmatic interactions as recorded in plagioclase phenocrysts of Chaos Crags, Lassen Volcanic Center, California. Journal of Petrology, 40(5) : 787–806.

Toummite, A., Ikenne, M., and Beraaouz, E.H., 2012. Geothermobarometry of Askaoun pluton in Ouzellarh-Sirwa promontory (central Anti-Atlas; Morocco). Open Journal of Geology, 2(03): 136.

Van der Zwan, F.M., Chadwick, J.P., and Troll, V.R., 2013. Textural history of recent basaltic-andesites and plutonic inclusions from Merapi volcano. Contributions to Mineralogy and Petrology, 166: 43–63.

Verdel, C., Wernicke, B.P., Hassanzadeh, J., and Guest, B., 2011. A Paleogene extensional arc flare‐up in Iran. Tectonics, 30(3): xxx–xxx.

Vernon, R.H., 1984. Microgranitoid enclaves in granites-globules of hybrid magma quenched in a plutonic environment. Nature, 309(5967): 438.

Viccaro, M., Ferlito, C., Cortesogno, L., Cristofolini, R., and Gaggero, L., 2006. Magma mixing during the 2001 event at Mount Etna (Italy): effects on the eruptive dynamics. Journal of Volcanology and Geothermal Research, 149: 139–159.

Whitney, D.L., and Evans, B.W., 2010. Abbreviations for names of rock-forming minerals. American Mineralogist, 95(1): 185–187.

Yang, H., Ge, W., Zhao, G., Dong, Y., Xu, W.L., Ji, Z., and Yu, J., 2015. Late Triassic intrusive complex in the Jidong region, JiamusieKhanka Block, NE China: geochemistry, zircon UePb ages, Lu–Hf isotopes, and implications for magma mingling and mixing. Lithos, 224–225: 143–159.

Yang, J.H., Wu, F.Y., Chung, S.L., Wilde, S.A., and Chu, M.F., 2006. A hybrid origin for the Qianshan A-type granite, northeast China: geochemical and Sr–Nd–Hf isotopic evidence. Lithos, 89(1–2) : 89–106.

Yang, X.M., and Lentz, D.R., 2005. Chemical composition of rock-forming minerals in gold-related granitoid intrusions, southwestern New Brunswick, Canada: implications for crystallization conditions, volatile exsolution, and fluorine-chlorine activity. Contributions to Mineralogy and Petrology, 150(3): 287–305.

Zingg, T., 1935. Beitrag zur schotteranalyse (Doctoral dissertation, ETH Zurich).

About the first author

Davood RAEISI, Male; born in 1985 in Kazerun City, Fars Province; Iran. PhD; research assistant of the Faculty of Science, University of Tehran; he is now interested in the study of Crystal Size Distribution (CSD), Petrogenesis of granitoids rocks and Metallogeny of the Tethyan Orogen. Email: d.raeisi@ut.ac.ir.

About the corresponding author

Prof. Hassan MIRNEJAD graduated with a Ph.D. degree in Geology from Carleton University, Ottawa, Canada in 2001. He was subsequently employed by the Geological Survey of Canada as a stable isotope analyst. Dr. Mirnejad moved to the University of Tehran in 2006 and was promoted to associate professor in 2011. He has also been an adjunct associate professor at Miami University, Ohio, since 2014. Dr. Mirnejad's research interests are isotope geochemistry, petrology of igneous rocks and ore deposits. E-mail: hmirnejad@ut.ac.ir